https://doi.org/10.5194/egusphere-2026-4617
Preprint. Discussion started: 25 August 2026

Fast online characterization of novel VOC permeation tubes by TD-GC-FID: Direct quantification via the effective carbon number concept

Ali Ghaddar[1,2], Mathilde Mascles[2], Jean-Philippe Amiet[2], Damien Bazin[2], Stéphane Le Calvé[1]
[1]Institute for Chemistry and Processes for Energy, the Environment and Health (ICPEES), UMR 7515, CNRS/University of Strasbourg, Strasbourg, 67087, France.
[2]Chromatotec, Saint-André-de-Cubzac, 33240, France.

Correspondence to: Stéphane Le Calvé (slecalve@unistra.fr)

Abstract. In atmospheric measurements, reliable calibration of analytical instruments used to monitor the concentrations of volatile organic compounds (VOCs) is achieved by means of traceable calibration standards. Permeation technology provides a flexible and continuous source of gaseous standards at trace levels; however, its application is not widespread for atmospherically-relevant VOCs, and the characterization remains limited to time-consuming gravimetric methods.
A comprehensive on-line and rapid thermodesorption-gas chromatography-flame ionization detector (TD-GC-FID) method was adapted after coupling with a dynamic generation system that housed four permeation tubes (PTs) containing benzene, *(E)*-2-hexenal, 2-methyl-1-butanol, and D-limonene–three of which are used for the first time in permeation. Emission rates (ERs) were determined for each PT over a total temperature range between 25 and 120 °C. At 35 °C, the ERs were 461±70 (±2σ) ng min^{-1}, 1721±74 ng min^{-1}, 723±103 ng min^{-1}, and 3.4±0.4 ng min^{-1} for benzene, *(E)*-2-hexenal, 2-methyl-1-butanol, and D-limonene. Experimental ERs varied between 288–1076 ng min^{-1} (25–50 °C) for benzene, between 1214–2022 ng min^{-1} (25–40 °C) for *(E)*-2-hexenal, between 346–1022 ng min^{-1} (25–45 °C) for 2-methyl-1-butanol, and between 3.4–1628 ng min^{-1} (35–120 °C) for D-limonene. The effective carbon number (ECN) approach was employed to calculate the response factors on FID for the simple and fast quantification of the generated concentrations. Generated concentrations for an overall total dynamic flow of zero-air between 200- and 536.4-mL min^{-1} were in the ranges of high ppb, 150–1358 ppb, 496–2134 ppb, 158–1091 ppb, for benzene, *(E)*-2-hexenal, 2-methyl-1-butanol, and ranging from low to high ppb (1.2–1018 ppb) for D-limonene, under their respective investigated temperature conditions. The ER-temperature dependence was fully established and explained based on Antoine's vapor pressure law and Fick's law of diffusion with maximum correlation R^2>0.998 over the investigated temperature ranges. Apparent permeabilities were estimated for each PT VOC-membrane system, with values ranging between 10^{-13}–10^{-9} mol m^{-1} s^{-1} Pa^{-1}, equivalent to magnitudes of permeability coefficients. Finally, the proposed method was extensively compared with other conventional gravimetric, offline chromatographic, and spectroscopic methods.

1 Introduction

Atmospheric volatile organic compounds (VOCs) are key precursors in atmospheric chemistry. VOCs undergo photochemical oxidative reactions with major atmospheric oxidants–such as ozone (O_3), hydroxyl (OH), and nitrate (NO_3) radicals (Atkinson and Arey, 2003)—thereby influencing the atmospheric oxidative capacity, forming tropospheric O_3 and generating secondary organic aerosols (SOA) (Atkinson, 2000). Overall, these processes widely impact air quality, the climate and the Earth's radiative balance. Excluding methane, global VOC emissions are dominated by biogenic sources, accounting for approximately 90 % of the total emissions (Guenther et al., 1995; Sindelarova et al., 2014). Biogenic volatile organic compounds (BVOCs) emissions originate primarily from vegetation (Kesselmeier and Staudt, 1999), and fluctuate significantly with meteorological variables—such as temperature, drought, and solar radiation—as well as plant responses to herbivory and pathogen attacks (Peñuelas and Llusià, 2001). These plant emissions encompass a wide variety of chemical families dominated by terpenoids (> 70 % isoprene and monoterpenes), followed by oxygenated VOCs such as alcohols and carbonyls (Guenther, 2013; Kesselmeier and Staudt, 1999). Although most oxygenated VOC emissions are less abundant than terpenoids under baseline conditions, they increase substantially under plant stress (Seco et al., 2007).
Recently, plant VOCs/BVOCs have gained interest as early indicators for applications in precision agriculture and plant conservation, notably for identifying characteristic biotic attacks (Coatsworth et al., 2022). Consequently, advanced analytical tools capable of detecting trace-level plant VOCs (low ppb to ppt range) with high sensitivity, selectivity, and temporal resolution

https://doi.org/10.5194/egusphere-2026-4617
Preprint. Discussion started: 25 August 2026

are required. Significant progress in portable, transportable, and near/real-time techniques–including gas chromatography with flame ionization detector (GC-FID) (De Blas et al., 2011), mass spectrometry (GC-MS) (Amiet et al., 2018; Bachelier et al., 2024), and photoionization detector (GC-PID) (Lara-Ibeas et al., 2019; Li et al., 2021; Liaud et al., 2014)—as well as proton-transfer-reaction mass spectrometry (PTR-MS) (Braun et al., 2025; Maleknia et al., 2007), Fourier-transform infrared spectroscopy (FTIR) (Ketola et al., 2006), and differential optical absorption spectroscopy (DOAS) (Lee et al., 2005)—enabled sub-ppb detection limits with analysis times ranging from seconds to minutes. In contrast, offline GC methods (e.g., U.S. EPA Method TO-17) relying on sorbent tubes and subsequent thermal desorption (TD-GC-MS) often suffer from sample instability and potential compound loss during storage (U.S. Environmental Protection Agency (EPA), 1999).

Nevertheless, all quantitative analytical techniques require reliable gaseous calibration standards spanning from ppt to ppm levels. Pressurized gas cylinders are widely used but suffer from wall adsorption, chemical degradation during storage, limited shelf time, cumbersome deployment, and high cost–limitations that are particularly acute for high-boiling and reactive plant VOCs. Dynamic generation systems overcome these drawbacks by continuously producing fresh gaseous standards. For instance, dynamic dilution methods generate atmospherically relevant VOC concentrations via permeation through polymeric membranes at constant rates and temperatures, swept by a carrier gas (e.g., pure nitrogen or zero-air). In permeation tubes (PTs), liquid or solid analytes are sealed within polymeric enclosures (e.g., polytetrafluoroethylene (PTFE), polydimethylsiloxane (PDMS), polyfluoroalkoxy alkane (PFA), or low-density polyethylene (LDPE)). While commercial PTs are readily available for common pollutants (such as BTEX, halocarbons, or formaldehyde), custom-built PTs are required for challenging compounds like acetaldehyde, mercaptans, or oxygenated plant VOCs. The performance of a PT—quantified by its emission rate (ER)—depends on membrane characteristics, dimensions, tube geometry, operating temperature, and analyte physicochemical properties.

Various methods exist to calibrate the PT emission rates, including gravimetric, volumetric, coulometric, and manometric techniques. Gravimetric calibration–weighing the PT periodically on a microbalance or suspension balance to measure mass loss—is the standard reference method providing traceable standards (Knopf, 2001; O'Keeffe and Ortman, 1966; Purdue and Thompson, 1972; Scaringelli et al., 1970). However, it requires extended periods (days to weeks) to achieve measurable mass loss at a 95 % confidence level, ignores potential moisture sorption or composition changes, and typically characterizes the PT at only a single temperature. Manometric methods monitor absolute pressure changes to shorten calibration times (Dietz et al., 1974), while volumetric and coulometric methods determine ERs analytically or electrochemically (Cedergren and Fredriksson, 1976; Saltzman et al., 1971).

Alternative off-line methods use sorbent sampling followed by HPLC-UV or GC analysis (Aoyagi et al., 2017, 2025; Grandjean et al., 2024), but these remain discontinuous due to sampling and preparation steps. Continuous online characterization offers a superior alternative by directly monitoring concentration variations in real-time, tracking stabilization periods, and immediately determining ERs. To date, only Neri et al. (2006) have reported real-time chromatographic calibration of PTs, and no study has targeted oxygenated plant VOCs or BVOCs using this approach.

Quantitative analysis of complex atmospheric matrices is further complicated by the need for pure calibration standards for every target analyte. Flame ionization detectors address this challenge through their predictable, wide linear dynamic range and nearly universal response to hydrocarbons. Although FID response depends primarily on carbon number, heteroatoms reduce this response.

The effective carbon number (ECN) concept introduced by (Sternberg et al., 1962) and refined in subsequent studies (Jorgensen et al., 1990; Kállai et al., 2001; Kállai and Balla, 2002; Tong and Karasek, 1984) accounts for heteroatomic contributions to predict response factors. The ECN approach is particularly valuable when target analytes are unavailable in static cylinders (Faiola et al., 2012). However, its application to fast, versatile, permeation-based generation of plant VOCs remains limited. Combining ECN-

https://doi.org/10.5194/egusphere-2026-4617
Preprint. Discussion started: 25 August 2026

based quantification with permeation systems minimizes the reliance on commercial gas standards while providing a flexible calibration method.

In this work, we present a comprehensive approach for the design and characterization of custom-fabricated PTs containing atmospherically relevant plant VOCs/BVOCs. Four plant VOC PTs were investigated, three of which—belonging to the alcohol, aldehyde, and monoterpene chemical families—have not been previously reported as stable permeation standards. A portable, temperature- and flow-regulated gas generation system was developed for both laboratory and field calibrations of transportable/portable TD-GC-FID/PID devices. Characterization was performed using an autonomous on-line gas chromatographic technique (TD-GC-FID), enabling continuous monitoring under varied temperatures and flow rates, rapid evaluation of PT stability, and precise determination of temperature-dependent emission rates across a wide range of ER values (< 5 ng min^{-1} to > 2 µg min^{-1}). Furthermore, dynamic dilution was investigated using low carrier gas flows (< 1 L min^{-1}), highly relevant for field deployment. Apparent membrane permeabilities were estimated to relate mass transport processes to membrane-analyte interactions. Finally, the ECN concept was evaluated to extend FID quantification to additional plant VOCs without commercial gas standards. Overall, this work demonstrates how online GC measurements, combined with FID and the ECN concept, provide a flexible (temperature and flow adjustment), traceable (from low ppb to high ppm), and robust calibration strategy for atmospheric and plant VOCs observations.

2 Materials and methods

2.1 Chemicals and materials

Benzene (purity≥99 %), *(E)*-2-hexenal (98 %), 2-methyl-1-butanol (≥99 %), and D-limonene (97 %) were purchased from Sigma-Aldrich. The chemical families and physical properties of each investigated compound are detailed in Table S1.

For the calibration of the TD-GC-FID instrument, a certified PAMS-58 gas mixture cylinder (Takachiho® Chemical Industrial Co., Japan, 100 ppb, nitrogen, 1000 L), containing 58 hydrocarbons (C2–C12 compounds), including benzene and monoterpenes, such as α- and β-pinene, was utilized. Carrier and dilution flows were controlled using three external mass flow controllers (MFC Bronkhorst, Montigny-lès-Cormeilles, France): two MFCs (0–100 mL min^{-1}) regulated the zero-air flow delivered through the two permeation ovens, respectively, while a third MFC (0–1000 mL min^{-1}) provided additional dynamic dilution with dry zero-air.

PTFE and stainless-steel tubing, PTFE and silicone membranes, and other mechanical components, including nuts, fittings, ferrules, and crimps, were all supplied by Chromatotec®, Saint-André-de-Cubzac, France. The mechanical components were used to clamp the corresponding membranes and to provide airtight and leak-tight sealing at the ends of the custom-built permeation tubes. Dry zero-air used as carrier gas and for dynamic dilution was produced by a zero-air generator (airmoPURE D, NMTHC < 0.1 ppb, Chromatotec®, Saint-André-de-Cubzac, France).

2.2 Design of the four permeation tubes

Four permeation tubes were fabricated from the four purchased analytical standards for benzene, *(E)*-2-hexenal, 2-methyl-1-butanol, and D-limonene, respectively. Figure 1 shows the different types of permeation tubes used in this work. Two permeation tubes (benzene and D-limonene) were adapted to a cylindrical configuration (radial configuration) with a permeable wall of a PTFE porous tubing, whereas the other two permeation tubes (*(E)*-2-hexenal and 2-methyl-1-butanol) followed a planar diffusion (axial diffusion) through a membrane perpendicularly capped onto an impermeable stainless-steel reservoir (see Fig. 1).

In the radial configuration (see Fig. 1a), around 1.2 mL of liquid analyte of benzene and D-limonene (approximately 2/3 of the internal volume of the tubing, and the remaining 1/3 for vapor build-up) where each contained inside an 8 cm-long (for D-limonene)

https://doi.org/10.5194/egusphere-2026-4617
Preprint. Discussion started: 25 August 2026

or a 10 cm-long (for benzene) PTFE tubing, with 1/4" or 6.35 mm outer diameter (OD), and 4.35 mm inner diameter (ID), giving a thickness δ of 1 mm. All dimensions were measured using a digital caliper with a 0–150 mm measuring range and 0.01 mm resolution. The permeation tube lengths were selected to fit within the maximum dimensions of the three permeation ovens (length: l_{max} = 18 cm) designed by Chromatotec® (see Fig. 1). The two ends of the PTFE tubing were trimmed beforehand for precision to a length of 8 cm or 10 cm. After securing two metallic crimps around the two ends using a tube flaring bar and a bench vice, two stainless-steel end fittings (hardened pins) were inserted into the ends and then retightened using the bench vice. Two neat indentations on both left and right sides of the outer crimps marked the proper tightening and sealing of the radial permeation tubes (see Fig. 1a). After sealing, the effective or exposed lengths over which the permeation occurred were around 5.5 cm for both benzene and D-limonene permeation tubes.

In the axial configuration (see Fig. 1b), the 10 cm-long permeation tube consists of a stainless-steel reservoir tank containing around 1–1.2 mL of liquid analyte (*(E)*-2-hexenal or 2-methyl-1-butanol). One end of the filled tank was fitted with a 1/4" stainless-steel nut fitting and ferrule that was connected to a 1/4″–1/8″ reducing union. On the other end of the union, a 1/8" stainless-steel ferrule and nut were fitted, which secured two stacked permeable membranes of PDMS (blue) and PTFE (white) on top (diameter = 3 mm, thickness of 2 mm for both) (see Fig. 1b). The PTFE membrane was pierced in the middle (diameter = 0.5 mm). The effective permeation diameter is then defined by the 3.27 mm inner diameter of the 1/8" compression nut. After mechanical tightening, the effective length of the tubing was 6.2 cm, measured using the caliper.

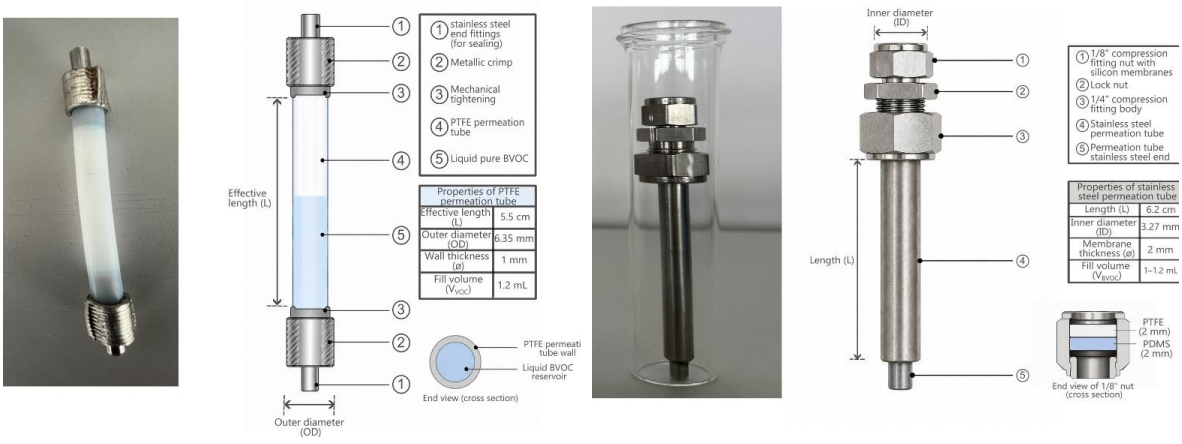

(a) **(b)**

Figure 1. (a) Original design of the custom-designed PTFE benzene and D-limonene permeation tubes (left), along with their schematic representation showing the PTFE permeation tube parts, properties, and principal dimensions (right). **(b)** Original design of the custom-designed stainless-steel *(E)*-2-hexenal and 2-methyl-1-butanol permeation tubes (left), along with their schematic representation showing the stainless-steel permeation tube parts, properties, and principal dimensions (right).

2.3 Gas generation apparatus

The characteristics of the four permeation tubes were evaluated using the gas generation setup described in Fig. 2. The setup features a dry zero-air generator, three mass flow controllers (MFCs), three temperature-controlled aluminum permeation ovens (each with a zero-air inlet and mixture outlet), a mixing chamber, an online TD-GC-FID system used as a real-time monitoring gas chromatograph, and an external pump for sampling.

Two permeation ovens out of the three were placed in series. One oven housed either benzene and *(E)*-2-hexenal permeation tubes at a regulated temperature interchangeably, while the second oven was regulated at a higher temperature, with the D-limonene permeation tube positioned inside. The second oven was placed in a larger isothermal heated chamber at 60 °C to ensure further

https://doi.org/10.5194/egusphere-2026-4617
Preprint. Discussion started: 25 August 2026

stability of the temperature. The third oven was externally added in parallel to the two ovens in series, and housed the 2-methyl-1-
150 butanol permeation tube at a different temperature. The temperatures were regulated through the automatic control of the gas generation system software and were previously validated manually using a digital thermometer equipped with a K-type thermocouple (Model 1310, TES Electrical Electronic Corp., Taipei, Taiwan) before each analysis within ±0.1 °C. Dry zero-air (regulated at 2 bar) flushed the three permeation ovens continuously at modulated flow rates (oven #1 and oven #2, with MFC 1 set at 62±1.2 mL min^{-1}, and external oven #3 with MFC 3 set at 68.0±1.34 mL min^{-1}). Both MFC 1 and MFC 3 have a range of
155 0–100 mL min^{-1}. MFC 2 (range 0–1000 mL min^{-1}) was used to dilute the two combined outputs of the three ovens (2 in series, 1 in parallel; see Fig. 2). The selected combined flow rates (sum of MFC 1, MFC 2, and MFC 3) for analysis were 288.20±12.96 mL min^{-1}, 386.97±13.22 mL min^{-1}, and 536.40±13.61 mL min^{-1} (for temperature of 25, 30, 40, 45, 50, 80, 90, 100, and 120 °C), and 200±12.73 mL min^{-1}, 314.04±13.03 mL min^{-1}, and 468.5±13.43 mL min^{-1} (for temperatures of 35, 90, and 110 °C).

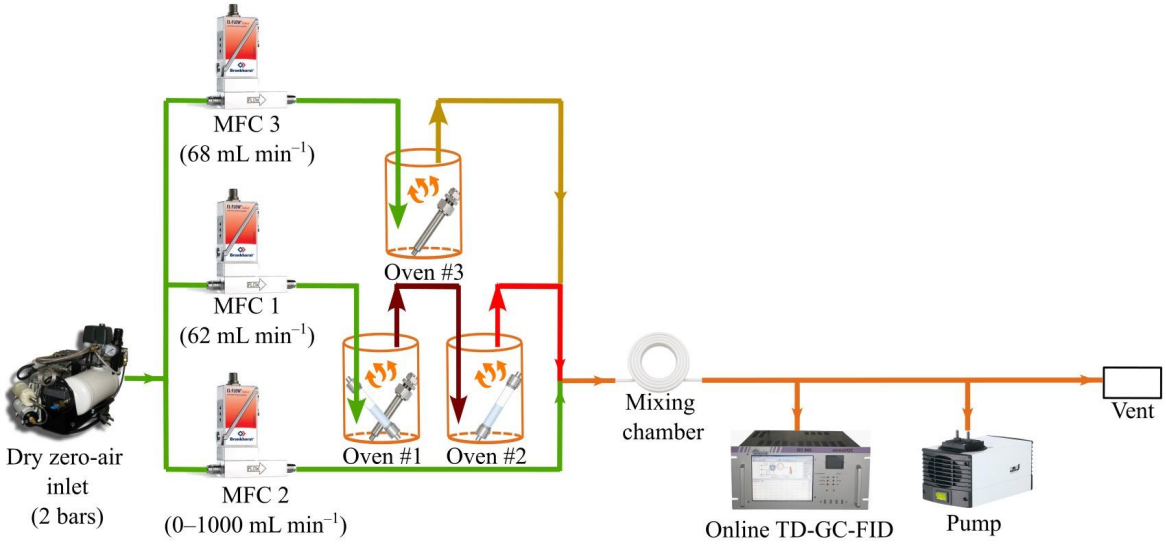

160 **Figure 2.** Schematic of the gas generation system designed for the generation of the target VOCs in this work.

2.4 Real-time monitoring of the gaseous mixture

The combined flow output of the mixture was eventually homogenized in a PTFE mixing chamber (3 m, 6 mm OD, 4 mm ID). The concentrations of the permeation tubes' gas-phase mixture at the outlet of the generation system were subsequently measured after dilution and mixing by means of a reference gas chromatograph (TD-GC-FID, airmoVOC C6–C12, Chromatotec®, Saint-
165 André-de-Cubzac, France) (see Fig. 2). The TD-GC-FID analyzer was calibrated prior to the experiments using a PAMS-58 cylinder and operated at a room temperature of 22±2 °C. Ultra-pure hydrogen (99.99 %), supplied via a hydrogen generator (Hydroxychrom, Chromatotec®, Saint-André-de-Cubzac, France), was used as the carrier gas and fuel for the FID detector, along with zero-air to sustain the FID flame. An external pump was used to sample the mixture output from the gas generator, delivering it to the analyzer while flushing the excess flow into the vent (see Fig. 2).

170 Continuous real-time measurements were carried out using the TD-GC-FID analyzer. The analyzer operated first by trapping the sample of the gaseous mixture on a sorbent tube made up of Carbopack adsorbents. The sample was drawn at ambient temperature and a flow rate of 19.9 mL min^{-1} in 22.5 minutes (equivalent to a ≈450 mL sampling volume), followed by a 4-min-long thermodesorption at 380 °C with a hydrogen flow of 3 mL min^{-1}. After thermodesorption, the sample was then injected into a non-polar MXT30CE column (30 m × 0.28 mm ID × 1µm film thickness; Chromatotec, France) at a constant hydrogen flow of 3 mL

https://doi.org/10.5194/egusphere-2026-4617
Preprint. Discussion started: 25 August 2026

min^{-1}. An oven temperature gradient was employed from 36 °C to 200 °C, with a gradual ramp to a final hold at 200 °C for 4.5 minutes before cooling at the end of the analysis. The compounds of the gaseous mixture were separated in 30 minutes. The FID temperature was set at 170 °C (hydrogen and zero-air flows of 26.8±0.5 and 176±2.4 mL min^{-1}, respectively).

Compound identification based on the NIST library was validated by coupling the TD-GC-FID to a single-quadrupole mass spectrometer (DET QMS, Chromatotec®, Saint-André-de-Cubzac, France) during a limited number of confirmatory experiments.

2.5 Quantitative analysis by flame ionization detector

2.5.1 Concentration determination

For each separated compound VOC_i, the concentration C_{VOC_i} (in mg m^{-3}) was calculated based on Eq. (1):

$$C_{VOC_i} = k_{VOC_i} \times A_{VOC_i} \quad (1)$$

where k_{VOC_i} (in ng mL^{-1} au^{-1}) is the calibration quantification factor and A_{VOC_i} (in au) is the peak area in arbitrary units.

The factor k_{VOC_i} relates the concentration of the compound to the peak area by incorporating several determining parameters according to Eq. (2):

$$k_{VOC_i} = \frac{RF_{VOC_i}}{S \times V} \quad (2)$$

where RF_{VOC_i} is the analyte response factor accounting for FID-dependent linear sensitivity, S (in au ng^{-1}) is the FID sensitivity, defined by the chromatographic signal per unit of mass of analyte, and V is the volume sampled through the adsorbent trap (in mL).

Relative response factors for each investigated compound in this work were estimated based on the concept of the effective carbon number (ECN). ECN represents the number of carbons in the investigated molecule, to which the FID can respond effectively in comparison to its aliphatic counterpart molecule (excluding all heteroatoms such as oxygen or nitrogen, and halogens). Scanlon and Willis (1985) defined the basis for calculating a relative response factor for GC-FID quantification. Accordingly, RF_{VOC_i} is related to the effective carbon number of the investigated molecule ECN_{VOC_i} through Eq. (3):

$$\frac{RF_{VOC_i}}{RF_{ref}} = \frac{M_{VOC_i} \times ECN_{ref}}{M_{ref} \times ECN_{VOC_i}} \quad (3)$$

where RF_{ref} is the experimentally determined response factor of the reference compound (e.g., benzene or toluene for the TD-GC-FID), M_{VOC_i} and M_{ref} (in g mol^{-1}) are the molecular weights of both the compound VOC_i and the reference compound, respectively, while ECN_{VOC_i} and ECN_{ref} are their corresponding effective carbon numbers.

ECN_{VOC_i} is calculated using Eq. (4):

$$ECN_{VOC_i} = \sum CC + \sum FC \quad (4)$$

where $\sum CC$ is the sum of the contributions of all carbon atoms in VOC_i chemical structure, and ($\sum FC$).is the sum of coefficients to correct for all contributions of the present functional groups in its chemical structure. For the reference compound (in this work, benzene), ECN_{ref} is equal to 6, corresponding to 6 carbon atoms (ECN reduction is zero for aromatic functional groups) as tabulated by Sternberg et al. (1962). The theoretical ECN values for all investigated compounds of choice and their relative response factors are shown in Table S2.

2.5.2 Emission rate determination

After determination of the generated gaseous concentration derived from the TD-GC-FID response through Eq. (1), the permeation tube emission rate ER_{VOC_i} (in ng min^{-1}) was calculated using Eq. (5) according to the concentration–total flow relationship:

https://doi.org/10.5194/egusphere-2026-4617
Preprint. Discussion started: 25 August 2026

$$ER_{VOC_i}(T) = C_{VOC_i} \times F_T \times 10^{-3} \quad (5)$$

where F_T is the total flow after dilution sent to the TD-GC-FID (mL min^{-1}) and C_{VOC_i} is expressed in µg m^{-3}.

A conversion factor K is usually used in atmospheric measurements to express the concentrations/emissions in units of mixing ratios in ppb. When introducing this factor into Eq. (5), Eq. (6) converts the concentration unit of C_{VOC_i} from mg m^{-3} into ppb:

$$ER_{VOC_i}(T) = C_{VOC_i} \times F_T \times K = C_{VOC_i}(ppb) \times F_T \times \frac{M_{VOC_i}}{24.04 \times 10^3} \quad (6)$$

where $C_{VOC_i}(ppb)$ is the concentration of the compound VOC_i in ppb (ng/g) and 24.04×10^3 represents the molar volume in mL mol^{-1} calculated at 20 °C and under atmospheric pressure (1 atm) using the TD-GC-FID analyzer convention.

3 Results and discussion

3.1 Temporal stability of generated concentrations of the investigated VOCs

Generated VOC concentrations were continuously monitored using online TD-GC-FID at a temporal resolution of 30 min after placing each permeation tube (PT) into its respective, temperature-regulated oven (Fig. 1). Online measurements were initiated following a 24 h thermal equilibration period for each PT upon oven placement.

To account for slight variations in manufacturing, the two PTFE PTs of benzene and D-limonene (manufactured on March 1, 2024) were fabricated prior to the two stainless-steel PTs of *(E)*-2-hexenal and 2-methyl-1-butanol (manufactured on March 8, 2024). Initially (t=0), the benzene PT was placed in oven #1 at 50 °C. During the first four days, the benzene concentration increased steadily, stabilizing approximately at 2 ppm at the end of the sixth day (March 6, 2024). Once benzene reached this level, testing of the D-limonene PT was initiated at 50 °C (t = 5 days).

To prevent detector saturation from high initial emission rates, the stainless-steel PTs containing *(E)*-2-hexenal and 2-methyl-1-butanol were initially maintained at 35 °C in ovens #1 and #3, respectively, under a total zero-air flow of 288 mL min^{-1}. Both tubes achieved steady-state emissions after 14 days (Fig. S1) with stabilized concentrations of approximately 855 ppb for 2-methyl-1-butanol and 1890 ppb for *(E)*-2-hexenal.

Temporal stability profiles recorded over 3 consecutive days across three dilution flow rates are illustrated in Fig. 3 for benzene, (*E*)-2-hexenal, and 2-methyl-1-butanol at 25 °C, and for D-limonene at 80 °C. Equivalent concentration profiles obtained at other temperatures (30, 35, 40, 45, 50, 90, 100, 110, and 120 °C) are provided in Fig. S2, while Fig. S3 details D-limonene emissions at lower temperatures (35–50 °C).

https://doi.org/10.5194/egusphere-2026-4617
Preprint. Discussion started: 25 August 2026

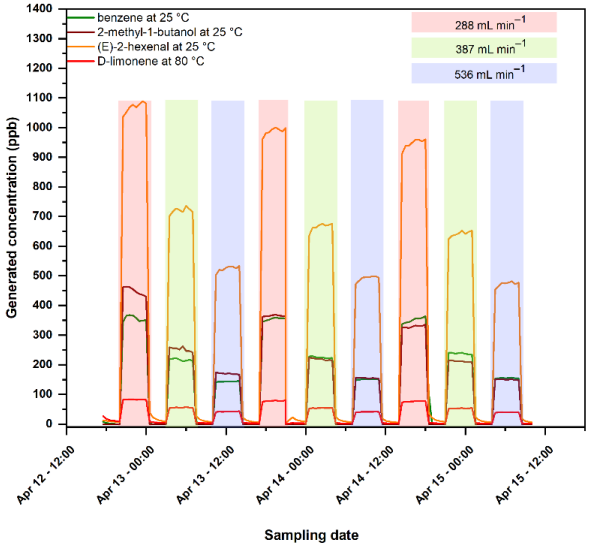

Figure 3. Concentration time profiles across different flow rates (n = 3 replicates) measured by online TD-GC-FID for benzene, 2-methyl-1-butanol, *(E)*-2-hexenal, and D-limonene at 25 °C for benzene, 2-methyl-1-butanol, and *(E)*-2-hexenal, and 80 °C for D-limonene. Shaded areas highlight the total dry zero-air dilution flow rates set by the three mass flow controllers (288 mL min^{-1} in red, 387 mL min^{-1} in light green, and 536 mL min^{-1} in blue). Blank measurements (n = 4) were systematically collected between continuous sequences (n = 8).

Detailed generated concentrations for all four compounds across investigated temperatures and flow rates are summarized in Tables S3–S6. Intermediate precision evaluated over multiple consecutive days (24 measurements at 25 °C and 80 °C) yielded relative standard deviations (RSDs). Overall, the PTFE PTs filled with benzene and D-limonene exhibited superior stability and lower RSDs, i.e., within 20 % across the investigated flow rate range, whereas RSD values of the two stainless-steel PTs concentrations exceeded 20 %. For instance, mean concentrations of benzene and 2-methyl-1-butanol were equal to 348±20 (RSD = 5.8 %, n=24) and 673±288 ppb (RSD = 42.7 %, n=24) at a flow rate of 288.2 mL min^{-1} and temperature of 30 °C. The higher variability observed for the stainless-steel PTs could not be unambiguously identified but could be is likely attributed to compound-specific physicochemical properties, such as differences in volatility, permeation dynamics, or potential adsorption/desorption losses along the sampling and injection lines.

3.2 Determination and repeatability of emission rates of the investigated VOCs

The generated concentration from each PT C_{VOC_i} (ppb) is related to the total combined flow rate from the three MFCs F_T (in mL min^{-1}) by the rearranged form of Eq. (6) (see Sect. 2.5.2). If Eq. (6) is rearranged, C_{VOC_i} (ppb) is expressed in terms of the emission rate of the PT $ER_{VOC_i}(T)$, in ng min^{-1}. By fitting a linear regression (C∝1/F) of these concentrations versus the inverse of the total flow rates ($1/F_T$) in 10^3 mL min^{-1}, the value of $ER_{VOC_i}(T)$ would be calculated by the following expression for each VOC_i:

$$ER_{VOC_i}(T) = slope(T) \times \frac{M_{VOC_i}}{24.04} \quad (7)$$

The results of the generated concentrations as a function of the inverse of the total flow rate are plotted in Fig. S3 for each investigated compound. For benzene, the emission rates were 306.4±20.6, 310.3±15.0, 497.1±32.8, 900.8 ±49.4, 962.7±25.4, and 1211.9±48.0 ng min^{-1}, at temperatures 25, 30, 35, 40, 45, and 50 °C, respectively. The uncertainty in the emission rate is calculated by considering the expanded standard error of the slope (±2σ) and error propagation according to Eq. (6). The emission rates for

https://doi.org/10.5194/egusphere-2026-4617
Preprint. Discussion started: 25 August 2026

the stainless-steel PT of *(E)*-2-hexenal at temperatures of 25, 30, 35, and 40 °C were 1063.9±174.4, 1426.7±165.8, 1737.7±41.2, and 2003.5±67.2 ng min^{-1}, respectively. For 2-methyl-1-butanol, the emission rates were in a range similar to the former PT, reaching 364.5±41.8, 613.5±155.8, 757.1±39.6, 1034.9±162.2, and 1063.9±137.8 ng min^{-1} at temperatures of 25, 30, 35, 40, and 45 °C, respectively. Finally, for the PTFE D-limonene PT, the emission rates were 3.39±0.24, 4.41±0.18, 6.10±0.18, 9.46±0.22, 125.3±4.1, 236.0±6.9, 465.2±27.0, 929.1±20.6, 1630.0±75.7 ng min^{-1} at 35, 40, 45, 50, 80, 90, 100, 110, and 120 °C, respectively. When fitting an inverse first-order model of concentration versus total flow rate, the resulting slopes were similar to those obtained from the linear fit ($C \propto 1/F$) for all the PTs (see Fig. S4). Experimental emission rates across varying flow rates and temperatures were calculated directly from the concentrations measured by TD-GC-FID. The emission rates for benzene, *(E)*-2-hexenal, 2-methyl-1-butanol, and D-limonene, are plotted against the total combined flow rate across the investigated temperature range (25–120 °C) in Fig. 4. Between each flow change made by the diluting MFC2 as well as prior to the initial setpoint, at least 4 blank chromatograms were recorded on the TD-GC-FID to evaluate potential memory effect. Peak area ratios for each compound VOC_i in zero-air blanks relative to the target chromatograms remained below 0.5 %, validating the effective flushing of both the sampling lines and the adsorbent trap.

https://doi.org/10.5194/egusphere-2026-4617
Preprint. Discussion started: 25 August 2026

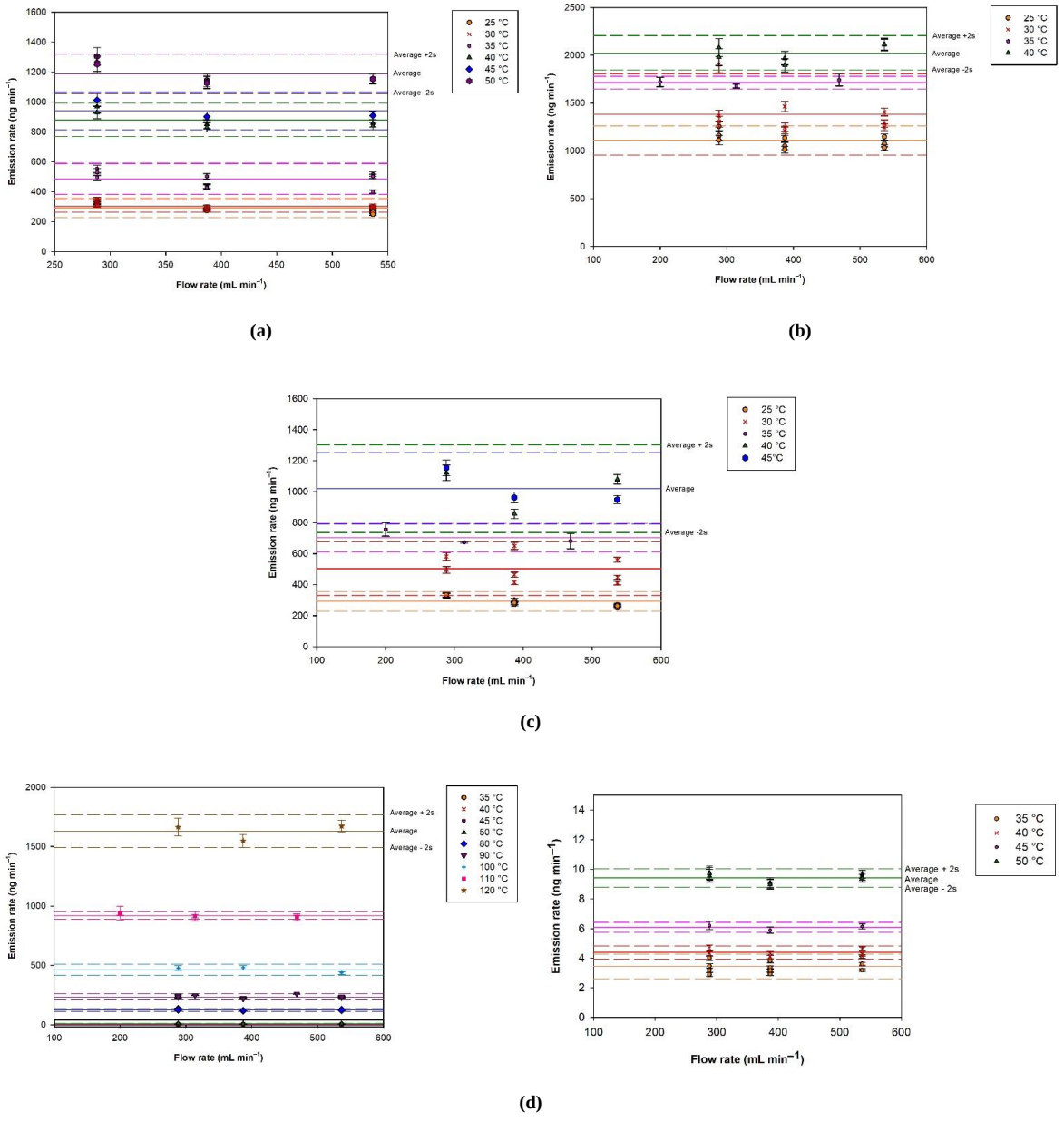

Figure 4. Emission rate (in ng min^{-1}) of **(a)** benzene permeation tube at 25, 30, 35, 40, 45, and 50 °C; **(b)** *(E)*-2-hexenal permeation tube at 25, 30, 35, 40 °C; **(c)** 2-methyl-1-butanol permeation tube at 25, 30, 35, 40, 45 °C; **(d)** D-limonene permeation tube at 35, 40, 45, 50, 80, 90, 100, 110, and 120 °C (left) with an enlarged view of the set of data recorded at 35, 40, 45, and 50°C (right) under dry zero-air total flow rates of 200, 314, and 469 mL min^{-1} (at corresponding temperatures of 35, 90, and 110 °C) and 288, 387, and 536 mL min^{-1} (at corresponding temperatures of 25, 30, 40, 45, 50, 80, 100, and 120 °C, rounded values for clarity), respectively. The horizontal solid lines represent the average emission rates, while the dashed lines indicate the average ± 2 standard deviations (average ± 2s). Vertical error bars represent the uncertainty of each measurement calculated from the propagation of the individual errors of the combined MFC1, MFC2, and MFC3 flows.

Experimental average emission rates for the benzene PT across all investigated temperatures in the range of 25–50 °C are presented in Table 1. Experimental data showed good agreement with the fitted emission rates (see Fig. S3a), with only minor deviations. For example, at 25 °C, the experimental average $ER_{benzene}$ was 287.6±34.9 ng min^{-1}, while the fitted value was 306.4±20.6 ng

https://doi.org/10.5194/egusphere-2026-4617
Preprint. Discussion started: 25 August 2026

min^{-1}, corresponding to a slight relatively limited difference of 6.54 %. The quoted errors of the experimental data represent the standard deviation of 3 replicate measurements collected under intermediate precision conditions (on different days). The experimental average emission rate data acquired over the investigated temperature and total flow rate ranges for the remaining compounds are summarized in Table S7–S9. Relative differences between fitted and experimental $ER_{(E)\text{-2-hexenal}}$ were 12.38 %, 2.97 %, 0.99 %, and 0.93 % at 25, 30, 35 and 40 °C, respectively, with noticeably higher differences at lower temperatures (close to ambient room temperatures of 21±2 °C). Good agreement was also obtained between fitted and experimental $ER_{2\text{-methyl-1-butanol}}$, with relative differences of 5.41 %, 8.64 %, 4.67 %, 1.48 %, and 4.14 % at 25, 30, 35, 40, and 45 °C, respectively. For D-limonene, relative differences between fitted and experimental $ER_{D\text{-limonene}}$ values varied between 0 and 4.13% across all flow rates and temperature conditions (0.29 % at 35 °C, 4.13 % at 40 °C, 0 % at 45 °C, 0.64 % at 50 °C, 0.84 % at 80 °C, 2.62 % at 90 °C, 0.32 % at 100 °C, 1.05 % at 110 °C, and 0.12 % at 120 °C). The standard deviations of averaged replicate measurements (intermediate precision) remained within 4–29 % for all the investigated compounds across all operating conditions. The error on individual experimental ER_{VOC_i} values at each flow and temperature condition was derived via error propagation based on the dominant expanded uncertainly of the three MFCs, which combines full-scale and reading-scale uncertainties according to Eq. (S1).

Table 1. Average emission rates of benzene at the investigated permeation oven temperatures (25, 30, 35, 40, 45, and 50 °C) and total dilution flow rates of MFC1, MFC2, and MFC3 (288.2, 387.0, and 536.4 mL min^{-1}). The table reports the mean emission rate ($ER_{benzene}$), relative standard deviation (RSD), and the total number of measurements (n_{total}) for each operating condition. The reported n_{total} includes all the measurements acquired over multiple experimental days (intermediate precision).

Flow (mL min^{-1})	**288.2**			**387.0**			**536.4**			
Temperature (°C)	$ER_{benzene}$ (ng min^{-1})	RSD[1] (%)	n_{total}[2]	$ER_{benzene}$ (ng min^{-1})	RSD (%)	n_{total}	$ER_{benzene}$ (ng min^{-1})	RSD (%)	n_{total}	Average±2σ (ng min^{-1})
25	325.6	0.7 %	24	280.2	4.7 %	24	256.9	3.9 %	24	287.6±69.9
30	314.9	5.8 %	24	277.8	3.4 %	24	291.3	2.3 %	24	294.7±37.6
35	501.0	5.6 %	24	433.6	8.9 %	24	450.2	13.5 %	24	461.6±70.2
40	888.6	2.9 %	16	787.1	1.7 %	16	793.9	1.5 %	16	823.2±113.5
45	903.6	4.6 %	16	818.1	2.0 %	16	844.9	1.3 %	16	855.5±87.5
50	1153.7	2.2 %	24	1028.8	0.8 %	24	1045.9	0.1 %	24	1076.1±135.4

[1] relative standard deviation. [2] total number of measurements for each operating condition.

3.3 Temperature dependence of emission rates

Given the dense nature of the polymeric membranes used in this work, for permeation to occur from the inside to the outside of the membrane, the process can only be explained by the solution–diffusion mechanism. In other words, the mechanism involves 4 steps: i) initial vaporization of the liquid (establishing the saturated vapor pressure internally); ii) solution (absorption and dissolving into the inner walls of the membrane); iii) molecular diffusion (movement) in and through the polymeric membrane due to a concentration gradient; and finally, iv) desorption from the outer walls of the membrane, entering, as a result, the gaseous mixture.

Concerning the first step, when attaining a liquid–vapor equilibrium of each compound *i* within the sealed PT at the operating temperature of the permeation oven, the inner partial vapor pressure of each compound *i* would be equal to the saturated vapor pressure. The saturated vapor pressure $P_{sat,i}(T)$ is a characteristic of each compound *i*, and it depends on the nature of the compound and the operating temperature, creating the thermodynamic driving force of the subsequent steps. The vapor pressure $P_{sat,i}(T)$ (in Pa) is calculated using the Antoine equation, Eq. (8):

$$\ln(P_{sat,i}) = A_i + \frac{B_i}{T} \quad (8)$$

https://doi.org/10.5194/egusphere-2026-4617
Preprint. Discussion started: 25 August 2026

where A_i and B_i are two empirical constants with units of pressure and temperature, and T is the operating temperature (in K). This step is typically fast in rate because excess liquid is available at the site of a much smaller vapor volume.

The second step involves the continuous collision of vapor molecules of VOC_i with the inner walls of the polymeric membrane, establishing rebound or dissolution-into-polymer effects. These effects define the affinity of the VOC_i toward the polymeric membrane under study. Once absorbed, Henry's law can be applied to explain the very small dissolved concentration of the VOC_i (solubility) in terms of the gaseous pressure after establishing the equilibrium with the polymeric membrane surface. Equation (9) defines this relationship based on Henry's law of partitioning:

$$C_S = \mathrm{S} \times \mathrm{p} \tag{9}$$

where C_S is the solubility/equilibrium concentration of the permeating gaseous VOC_i dissolved into the polymeric membrane (in mol m^{-3}), S is the solubility coefficient of VOC_i into the solid, similar to Henry's constant, which expresses the readiness of the VOC_i to dissolve into the polymer per unit pressure (in mol m^{-3} Pa^{-1}), and p is the partial pressure of VOC_i at the membrane interface.

The third step describes the molecular diffusion of the dissolved compound. Considering that the VOC_i is now molecularly dissolved into the polymeric membrane following sorption, the VOC_i molecules diffuse through the dense polymer membrane in the direction of a decreasing concentration gradient established between the two opposing inner and outer interfaces of the membrane. The mass transfer is expressed using Fick's first law of diffusion, which is the rate-limiting step. The law, defined by Eq. (10), states that the rate of the penetrant gas diffusion (diffusive flux) is directly proportional to the decreasing concentration gradient (from higher to lower concentration) under steady-state conditions:

$$J_i = -D_i \times \frac{dc_i}{dx} \tag{10}$$

where J_i is the diffusive flux of VOC_i (rate of transfer per unit area of section), D_i is the diffusion coefficient of the VOC_i within the membrane (in m^2 s^{-1}), and $\frac{dc_i}{dx}$ is the concentration gradient of VOC_i across the membrane.

Physically, the polymeric membrane has a thickness δ over which the analyte diffuses linearly under steady-state conditions. If this is assumed, the diffusion occurs mainly through a specific location (thickness), thus defining the variation of the concentration dC_S, across this thickness ($dx = \delta$). After substituting Eq. (9) into Eq. (10), Eq. (11) is established as:

$$J_i = -D_i \times \frac{dC_S}{\delta} = -D_i \times \mathrm{S} \times \frac{\mathrm{dp}}{\delta} \tag{11}$$

In the last step, and after the diffusion of VOC_i into the membrane, the dissolved VOC_i molecules desorb from the outer membrane surface of the membrane. Because dry zero-air is continuously flushing the PT membrane itself, VOC_i desorption is considered a fast process, in which the external partial pressure of VOC_i (P_{ext}) remains negligible/null. Equation (11) can be rewritten as Eq. (12):

$$J_i = -D_i \times \mathrm{S} \times \frac{[P_{ext} - P_{VOC}(T)]}{\delta} = D_i \times \mathrm{S} \times \frac{P_{VOC}(T)}{\delta} \tag{12}$$

The product of the diffusivity and solubility coefficients $D_i \times \mathrm{S}$ is defined as the permeability coefficient designated by Pr (T) (in mol m^{-1} s^{-1} Pa^{-1}). In most cases, the primary determinant of this coefficient among many complex variables (including the molecular weight of VOC_i, the amount of added impurities in the neighborhood of VOC_i, temperature, local electrical fields, etc.) is the nature of the polymeric membrane. The gas permeability through a polymeric membrane (in polymer science) is an intrinsic property of the used PT membrane–VOC_i system, and is often expressed in units of Barrer (1 Barrer = 10^{-10} cm^3(STP) cm^{-1} s^{-1} cm Hg^{-1}).

https://doi.org/10.5194/egusphere-2026-4617
Preprint. Discussion started: 25 August 2026

Since the membrane is homogeneous with a defined thickness δ under constant temperature and steady-state conditions, the emission rate $ER_{VOC_i}(T)$ is defined as the integral of the localized flux (in ng min^{-1}) over the effective permeation surface area A_{eff} (in m^2), and expressed by Eq. (13):

$$ER_{VOC_i}(T) = \int J \times dA_{eff} \quad (13)$$

The diffusive flux is expected to be uniform over the effective surface area. Adding every contribution of the flux over infinitesimal parts of the effective area typically simplifies the overall equation into a final Eq. (14), which establishes a relationship between the emission rate, the permeability, the effective area, the membrane thickness δ, and the vapor pressure of VOC_i at temperature T:

$$ER_{VOC_i}(T) = J \times A_{eff} = \Pr(T) \times \frac{P_{VOC}(T)}{\delta} \times M_{VOC_i} \times A_{eff} \times 60 \times 10^9 \quad (14)$$

Introducing the natural logarithm on both sides of Eq. (14) and after substituting Eq. (8) in the exponential form, Eq. (14) can be rewritten as Eq. (15):

$$lnER_{VOC_i}(T) = \ln(\Pr(T) \times \frac{e^{A+\frac{B}{T}}}{\delta} \times M_{VOC_i} \times A_{eff} \times 60 \times 10^9) = A' + \frac{B}{T} \quad (15)$$

where A' is the apparent pre-exponential constant or y-intercept relating $lnER_{VOC_i}(T)$ to $^1/_T$. This constant incorporates the temperature-dependent factors, including Antoine's constant A_i derived from the vapor pressure of VOC_i and the permeability coefficient Pr.

The values of the constants A' and B can be extracted after plotting the relationship of $lnER_{VOC_i}(T)$ versus $^1/_T$ over the temperature ranges for benzene (25–50 °C), *(E)*-2-hexenal (25–40 °C), 2-methyl-1-butanol (25–45 °C), and D-limonene (35–120 °C). Figures 5a, 5b, 5c, and 5d show the temperature dependence for each investigated VOC_i, respectively. The dependence of $lnER_{VOC_i}(T)$ on $^1/_T$ was adequately illustrated by a linear regression plot, resembling an Arrhenius-type relationship over the studied temperature ranges, with coefficients of determination (R^2) ranging from 0.922 to 0.998.

The following $lnER_{VOC_i}(T)$ versus $^1/_T$ regression equations for benzene, *(E)*-2-hexenal, 2-methyl-1-butanol, and D-limonene, respectively, are:

$$lnER(T) = -(6001 \pm 1608) \cdot \frac{1}{T} + (25.64 \pm 5.14)$$

$$lnER(T) = -(3124 \pm 196) \cdot \frac{1}{T} + (17.59 \pm 0.64)$$

$$lnER(T) = -(5059 \pm 1694) \cdot \frac{1}{T} + (22.94 \pm 5.48)$$

$$lnER(T) = -(9925 \pm 270) \cdot \frac{1}{T} + (30.88 \pm 0.78)$$

where the quoted errors represent twice the standard error on the regression slope and y-intercept (2σ). Ideally, a third Antoine constant C_i is typically inserted in Eq. (15) to correct for the experimental results as follows: $lnER_{VOC_i}(T) = A'_i + \frac{B_i}{T + C_i}$. However, the simpler two-parameter model was retained, since the inclusion of the third parameter was statistically insignificant (e.g., temperature range is small for *(E)*-2-hexenal and D-limonene, uncertainty on C_i by fitting a non-linear regression of the equation for benzene and 2-methyl-1-butanol, which is larger than the parameter C_i itself).

Using the retrieved slopes from the aforementioned equations, apparent activation energies E_a (in kJ mol^{-1}) can be calculated using the following Arrhenius-type equation (Eq. (16)):

$$lnER_{VOC_i}(T) = -\frac{E_a}{R} \cdot \frac{1}{T} + lnA'' \quad (16)$$

https://doi.org/10.5194/egusphere-2026-4617
Preprint. Discussion started: 25 August 2026

where R is the gas constant or 8.314 J mol^{-1} K^{-1}, and A'' is the pre-exponential Arrhenius factor, or the hypothetical emission rate at T_∞. The activation energy describes the energy barrier required to evaluate how rapidly the emission rate changes with temperature. The slope B combines the contributions from the membrane permeability and the investigated VOC_i vapor pressure at a temperature T, and can be assumed equal to $-\frac{E_a}{R}$ for the estimation of the apparent activation energy. Table S10 provides the values of B, E_a, and A'' for benzene, *(E)*-2-hexenal, 2-methyl-1-butanol, and D-limonene, respectively. At room temperature of 25 °C, benzene exhibits a much higher vapor pressure than D-limonene (VP of benzene 94.8 mmHg >> VP of D-limonene 2.33 mmHg, see Table S1). Owing to its high volatility and light size, a slight increase in the thermal energy is required to promote the transport and emission process of benzene from a radial PTFE membrane, in contrast to D-limonene emissions (E_a of benzene = 49.9±13.4 kJ mol^{-1} << E_a of D-limonene = 76.7±2.2 kJ mol^{-1}). Similarly, *(E)*-2-hexenal has a higher vapor pressure than 2-methyl-1-butanol at room temperature (VP of *(E)*-2-hexenal 4.11 mmHg > VP of 2-methyl-1-butanol 3.13 mmHg, see Table S1). For the case of the two stainless-steel reservoir PTs, *(E)*-2-hexenal showed a lower E_a (25.9±1.7 kJ mol^{-1}) than 2-methyl-1-butanol E_a (42.1±14.1 kJ mol^{-1}), suggesting a higher sensitivity-to-temperature characteristic for the case of 2-methyl-1-butanol within the studied temperature range. 2-methyl-1-butanol has a hydroxyl group (─OH), making the molecule more polar with lower affinity to the highly hydrophobic PDMS membrane. In contrast, *(E)*-2-hexenal is less polar with a carbonyl group (C=O), more hydrophobic, and likely to solubilize more readily into the PDMS membrane. This might explain why the emission process was easier to achieve for the case of *(E)*-2-hexenal than 2-methyl-1-butanol, regardless of the smaller molecular size and lower volatility properties of 2-methyl-2-butanol.

https://doi.org/10.5194/egusphere-2026-4617
Preprint. Discussion started: 25 August 2026

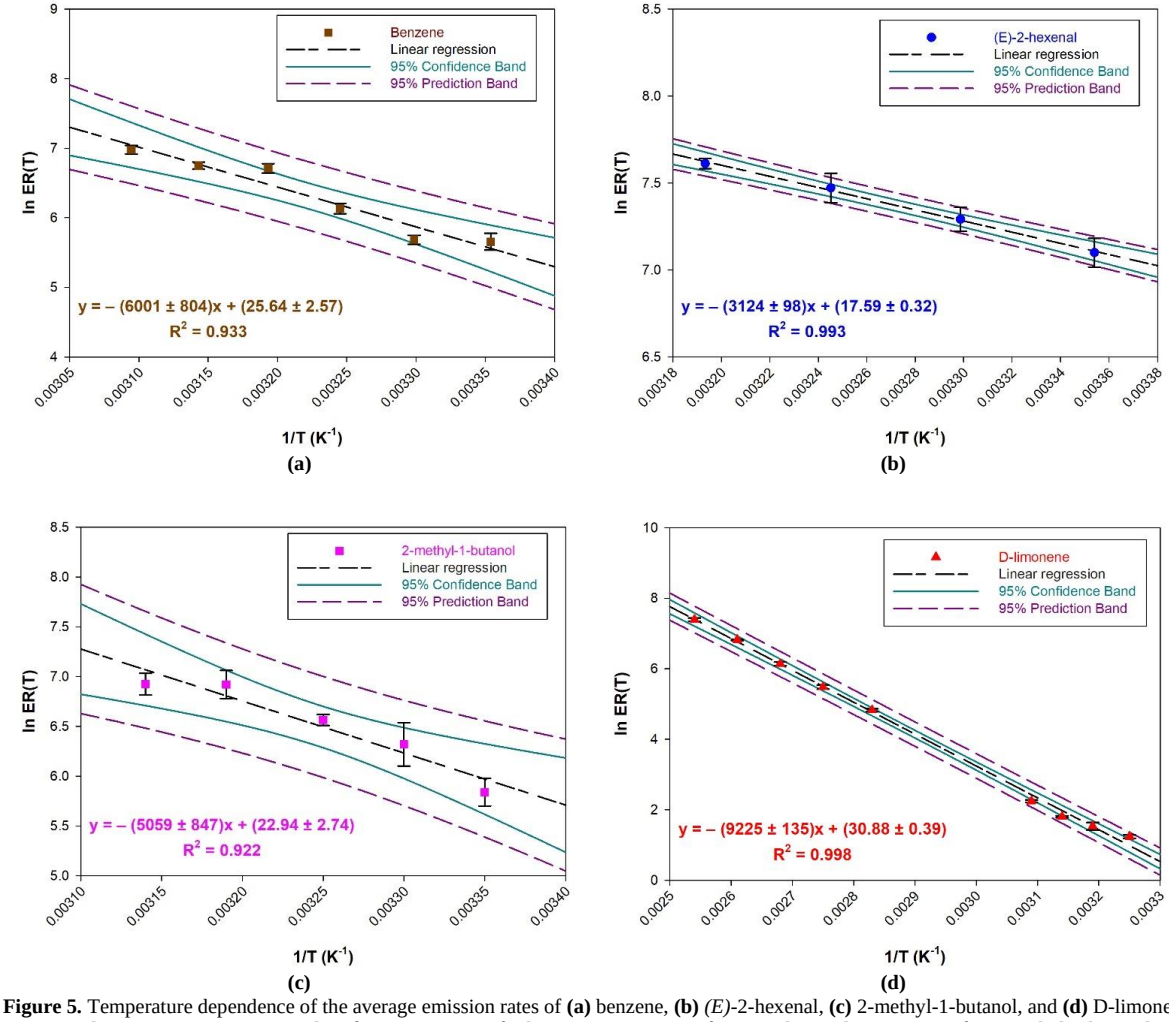

Figure 5. Temperature dependence of the average emission rates of **(a)** benzene, **(b)** *(E)*-2-hexenal, **(c)** 2-methyl-1-butanol, and **(d)** D-limonene over varied temperature ranges extending from 25 to 50 °C for benzene, 25 to 40 °C for *(E)*-2-hexenal, 25 to 40 °C for 2-methyl-1-butanol, and 35 to 120 °C for D-limonene. Vertical error bars represent the standard deviation of replicate mean values (n = 3), each calculated from the average of consecutive repeated measurements ($n_{minimum}$ = 8). The linear regression of the experimental data is expressed by the black dashed line. Uncertainty in the regression line is represented by the confidence band (region of 2 blue solid lines), while the expected range for future experimental data, accounting for both the uncertainty and variability of individual measurements, is represented by the prediction band (region of 2 purple dashed lines). The level of confidence was 95 %.

3.4 Concentration ranges of the four permeation tubes

The high correlation factors determined from the temperature dependence of emission rates ($lnER_{VOC_i}(T)$ versus $^1/_T$) are not merely descriptive (see Fig. 5a– d). By measuring the emission rate over a limited temperature window, it becomes possible to reliably interpolate and extrapolate these rates across an extended temperature range. Combining these predicted emission rates with the total dilution flow rates using Eq. (6) allows the calculation of the generated gas concentrations (in ppb) over a broad operational range without requiring any additional experimental data. Table S11 summarizes the concentration ranges achievable for the four target compounds within their respective temperature ranges.

https://doi.org/10.5194/egusphere-2026-4617
Preprint. Discussion started: 25 August 2026

To illustrate, consider the operational flow range combining fixed flows from MFC1 (62.3±1.21 mL min^{-1}) and MFC3 (68.0±1.34 mL min^{-1}) with MFC2 set at either its minimum (no dilution) or maximum capacity (1000 mL min^{-1}). For the benzene PTF PT, with an experimental emission rate ($ER_{benzene}$) of 461.6±70.2 ng min^{-1}, the resulting concentration range spans from 125.7 to 1092.8 ppb at 35 °C (see Table 1 and Table S11). In contrast, the D-limonene PTFE PT generated a narrow concentration range of only 0.5–4.6 ppb at 35 °C ($ER_{D\text{-}limonene}$ = 3.4±0.4 ng min^{-1}), representing a span of 4.1 ppb, compared to that exceeding 950 ppb for benzene.

This stark difference in concentration range magnitude—which persists at all investigated temperatures—is primarily driven by high vapor pressure and smaller molecular weight of benzene, providing a much stronger thermodynamic driving force of benzene across the PTFE membrane (see Table S1).

Furthermore, owing to the exponential temperature dependence of emission rates, raising the oven temperature significantly expands the accessible concentration ranges: i) For benzene PTFE PT, by increasing the oven temperature from 35 °C to 50 °C, the generated concentration range ($ER_{35\,°C}$ = 461.6±70.2 ng min^{-1} vs. $ER_{50\,°C}$=1076.1±135.4 ng min^{-1}) expanded the concentration range from 125.7–1092.8 ppb to 293.1–2547.6 ppb; ii) For the D-limonene PTFE PT, over the same temperature range where $ER_{35\,°C}$ = 3.4±0.4 ng min^{-1} and $ER_{50\,°C}$=9.4±0.7 ng min^{-1}, the concentration ranged from 0.5–4.6 ppb to 1.5–12.8 ppb (see Table S9).

In the case of the two stainless-steel PTs, operating over the same standard flow range at 35 °C yielded concentrations of 373–3242 ppb for *(E)*-2-hexenal (ER=1720.6±74 ng min^{-1}) and 174.6–1517.4 ppb for 2-methyl-1-butanol (ER=723.3±103 ng min^{-1}) (Table S7 and S8). Increasing the temperature from 25°C to 40°C for *(E)*-2-hexenal stainless-steel PT ($ER_{25\,°C}$ = 1214.2±197.2 ng min^{-1} vs. $ER_{40\,°C}$=2022.3±122.4 ng min^{-1}), expanded its generated concentration range from 263.2–2287.9 ppb to 438.4–3810.6 ppb, representing a 1.67-fold expansion in span. In comparison, a more pronounced 2.95-fold increase in concentration span was obtained for the 2-methyl-1-butanol stainless-steel PT when raising the temperature from 25 °C to 45 °C, ($ER_{25°C}$ = 345.8 ± 99.2 ng min^{-1} vs. $ER_{45°C}$ = 1021.6 ± 228.4 ng min^{-1}), widening the achievable concentration range from 83.4–725.4 ppb to 246.5–2143.1 ppb.

3.5 Comparison with literature

The designs and performance of the proposed PTs in this work were evaluated against existing permeation tube devices to demonstrate their applicability and versatility in aspects relevant to atmospheric and plant emission studies. Particular emphasis was placed on the calibration method, the membrane material, and PTs geometric configuration, permeability, repeatability, and the achievable range of generated concentrations.

To calibrate PTs and determine their emission rates, several approaches have been reported in the literature, including gravimetric mass-loss measurements (using either a high-resolution microbalance or a magnetic suspension balance), thermogravimetric analysis (TGA), offline sampling followed by chromatographic analysis, and spectroscopic methods such as UV spectroscopy. Table S12 compares representative permeation technologies reported in the literature. In the present work, the generated concentrations of the four target compounds (benzene, D-limonene, *(E)*-2-hexenal, and 2-methyl-1-butanol) were monitored along with the online determination of their emission rates under controlled operating conditions of carrier gas flow rate and oven temperature.

3.5.1 Conventional gravimetric calibration method versus the online TD-GC-FID based method

Most commercial PTs are characterized using the universal gravimetric calibration method defined by the standard ISO 6145 (International Organization for Standardization (ISO), 2002). The emission rate (ER) is obtained by periodic weighing of the PT (procedure ISO 6145-10), representing the slope of mass loss (Δm) versus time (Δt) once thermal equilibrium is reached. Due to

https://doi.org/10.5194/egusphere-2026-4617
Preprint. Discussion started: 25 August 2026

the extended weighing periods required by routine laboratory balances (spanning several days to months), thermostated microbalances are often used instead.

Pioneering work in permeation technology began in the 1960s with O'Keeffe and Ortman (1966), who introduced gravimetric calibration for trace gas generation using FEP Teflon tubing filled with liquefied gases or volatile liquids (propane, butane, SO_2, and NO_2). Over test periods of days to weeks (T = 13.8–29.1 °C in a water bath), they observed a normalized emission rate ranging from 27.1 to 2290 ng min^{-1} cm^{-1} (Table S12), along with operational issues such as a 10–15 % emission rate sensitivity to temperature fluctuations, moisture susceptibility, microscopic gas blistering, and polymer swelling.

Subsequent studies highlighted the constraints of gravimetric calibration across various chemical classes and membrane geometries. First, regarding Volatile Sulfur Compounds (VSCs), Beltz et al. (1986) demonstrated that calibrating gas-tight stainless-steel PTs (ER = 10–1000 ng min^{-1}) across 25–60 °C required a balance sensitivity of +/-100 ng. Stevens et al. (1969) required 6 weeks to calibrate FEP Teflon PTs (d = 0.762 and 5.08 mm) at 20.3 °C, observing higher relative uncertainties (3.5–4.0%) for low-emitting tubes (183 ng min^{-1} for H_2S) compared to high-emitting ones (1.7–2.3% for 1040 ng min^{-1} SO_2) (Stevens et al., 1969). Second, for halocarbons, by means of permeation in atmospheric applications, emission rates of earlier commercial PTs were validated using the gravimetric method by Singh et al. (1977). They evaluated commercial FEP PTs for 18 halocarbons of varying wall thicknesses (δ≈3.175, 0.762, and 1.575 mm) and of constant length (L≈8.13 cm) and weighed them at least once a week by means of a semi-micro balance (10^{-5} g mass resolution). Reported emission rates for PTs of these 18 halocarbons (maintained at T° = 31±0.05 °C and flushed with pre-purified helium gas) ranged from 64.8 ng min^{-1}±40.3 % (lowest, for CCl_2CCl_2) to 14160 ng min^{-1}±1.7 % (highest, for $CClF_2CClF_2$). Higher relative uncertainties were observed for low-emitting PTs for a precision of ±95 % confidence interval of slopes of mass loss versus time plots. In a similar study, Crescentini et al. (1981) suggested that at least two (~15 days) to six weeks are required to gravimetrically calibrate a group of halocarbon PTs (radial FEP Teflon, δ ≈ 0.3, 0.9, and 3 mm). In another work, a chlorinated VOC, vinyl chloride, was housed in an FEP Teflon PT, and its weight was periodically measured using a conventional balance (0.01 mg mass resolution) (Bankovich and Modrell, 1976). It was reported that a period of 9 months was required to obtain a mean vinyl chloride emission rate of 6.243±0.056 µg min^{-1} (6243±56 ng min^{-1}) at 30 °C±0.5 % under a flow rate of factory air of 100 mL min^{-1}. Third, for Aromatic Hydrocarbons (BTEX), Pérez Ballesta et al. (1999) recommended a minimum weighing window of >4 weeks for FEP and TFE BTEX PTs (FEP Teflon: L = 5–50 mm, δ = 0.762 mm; TFE: L = 20–100 mm, δ = 0.762 mm) with typical emission rates of ~20 and 100–400 ng min^{-1}, respectively, using a comparator mass balance with reported 8 µg standard deviation of repeated weighing. As summarized in Table S12, conventional gravimetric methods cover emission rates ranging from tens of ng min^{-1} to tens of µg min^{-1}, but demand extended testing times depending on the analyte, membrane materials, dimensions, and target concentration.

In contrast, the proposed on-line TD-GC-FID methodology developed in this work dramatically accelerates ER determination. For example, validating the ER of a single PT (such as benzene, 2-methyl-1-butanol, or *(E)*-2-hexenal) requires only ≈ 1.4 days (Fig. S1)— representing an approximate 22-fold reduction in calibration time compared to traditional gravimetric techniques. Furthermore, coupling the gas generation system directly to online TD-GC-FID eliminates major historical limitations of gravimetry, including: (i) Long conditioning and equilibration delays; (ii) Physical disturbances caused by repeatedly removing PTs from their thermal enclosures for weighing; (iii) Coarse temporal resolution (one data point every few days or weeks); (iv) Confounding humidity-absorption and permeation effects during handling, and (v) Uncharacterized or unquantified short-term emission rate fluctuations.

https://doi.org/10.5194/egusphere-2026-4617
Preprint. Discussion started: 25 August 2026

3.5.2 Thermogravimetric calibration method versus the online TD-GC-FID based method

As noticed in the aforementioned literature, and while providing high accuracy, the conventional gravimetric approach is time-consuming, labor-intensive, and its relative uncertainties are particularly evident for low-emission PTs due to the need for sufficient accumulation of mass loss over extended periods of time. Maria et al. (2002) employed thermogravimetry as a first alternative to periodic gravimetric weighing for the determination of emission rates of PTs. They fabricated a benzene PT (PTFE, L_{eff} = 11 mm, δ = 0.85 mm) and weighed it continuously (50 points × 24 h) using a thermobalance (0.2 µg resolution, 1 µg readability) at 31±0.2 °C under ≈8.3 mL min^{-1} nitrogen flow. They reported an overall validation of a ~20 ng min^{-1} steady-state emission rate after approximately 2 weeks (see Table S12).

In a later similar work, five laboratory custom-made BTEX PTs (PTFE, L = 20, 30, and 40 mm, δ = 0.8 mm) were calibrated continuously for a 120-h period using the same thermobalance set-up at 31±0.2 °C, yielding an emission rate range of 25.8–349.7 ng min^{-1} (±0.01–0.05 ng min^{-1}) (Tumbiolo et al., 2005). We demonstrate in this work a better temperature regulation of the permeation oven within ±0.1 °C, in addition to an enhanced manual sensing check of the oven temperature after each temperature change, thus avoiding the issues related to noise and uncertainty reported by Maria et al. (2002) and Tumbiolo et al. (2005). Tumbiolo et al. (2005) also reported a two-day stabilization period required after each change of operating conditions for the reliability of emission rates to be achieved. In this work, we report online real-time monitoring of the re-stabilization/re-equilibration of the generated concentrations of each investigated PT simultaneously, with observed re-stabilization of monitored concentrations after acquiring several blanks of dry zero-air for ≈ 2–3 hours of analysis. In addition, the thermogravimetric method assumes that the mass loss of the analyte corresponds entirely to the analyte itself, with no consideration of possible impurities that would otherwise require mass spectrometry or infrared spectroscopy for inspection (Tumbiolo et al., 2005), whereas the online TD-GC-FID method in this work considers the real-time study of the composition by investigating the chromatogram for additional peaks after identification.

3.5.3 Magnetic-suspension-balance gravimetric calibration method versus the online TD-GC-FID based method

While the thermogravimetric approach overcame several limitations associated with conventional gravimetric analysis, magnetic-suspension-balance (MSB) weighing introduced significant advancements, including higher resolution, enhanced sensitivity, continuous mass tracking, and non-mechanical coupling between the balance and the PT. Using continuous MSB (1 µg microbalance) and under controlled temperature conditions, Knopf (2001) calibrated an SO_2 PT (type and dimensions not reported), and validated an emission rate of 1.273 × 10^{-8} g s^{-1}±0.86 % (or 763.8 ng min^{-1}) via linear regression of mass loss versus time over 7 hours to 3 days. In brief, a relative standard uncertainty of ~0.9 % was achieved (expanded uncertainty <2 %, k = 2).

In a subsequent study, emission rates of commercial stainless-steel PTs containing halogenated greenhouse gases were determined via MSB at 45 °C. The resulting emission rates ranged from 88.5 to 1654.8 ng min^{-1} (see Table S12), with expanded uncertainties of 0.6–1.3 % (k = 2) after continuous monitoring for at least 22 days (Guillevic et al., 2018). Moreover, for atmospheric applications such as calibrating instruments with ammonia (NH_3), Macé et al. (2022) gravimetrically calibrated a commercial NH_3 PT (PTFE/FEP, 99.98 % purity) using the Borda weighing method (correcting for air buoyancy) on a microbalance (1 µg resolution) under 100 mL min^{-1} of dry zero-air at 30±0.05 °C. This yieldeda validated emission rate of 474.6±3.4 ng min^{-1} (k = 2), with temperature variations contributing 43.14 % to the total uncertainty over a 2-year evaluation period.

In contrast, the present work overcomes the inherent reliance on mass loss measurements in the MSB approach by providing direct chemical quantification and characterization of the gas mixture composition. Reliable operation of specialized metrological MSBs requires stringent control over temperature (±0.02 °C), air buoyancy, and signal drift, alongside operational constraints imposed by the weight and bulk of laboratory-bound balances. Furthermore, we demonstrate rapid characterization of emission rates within

https://doi.org/10.5194/egusphere-2026-4617
Preprint. Discussion started: 25 August 2026

comparable emission bounds (from tens to thousands of ng min^{-1}) in <22 days using a similar stainless-steel material to that of Guillevic et al. (2018).

3.5.4 Offline chromatographic calibration method versus the online TD-GC-FID based method

In addition to gravimetric methods for PT calibration, emission rates of PTs used for monitoring atmospheric pollutant concentrations have also been determined based on offline sampling of the generated VOC mixture followed by chromatographic analysis. Specifically, Susaya et al. (2011, 2012) and Kim et al. (2012) relied on an offline collection of PT-generated aromatic mixture (BTX and BTEX, respectively) into 10 L Tedlar® bags, followed by transfer onto Carbopack X adsorbent traps, thermal desorption, and finally, final quantification by GC-FID. Susaya et al. (2011) reported that determining emission rates (at 30 °C, under ultrapure nitrogen flows of 20–1200 mL min^{-1}) for commercial, high-emitting PTFE PTs (L = 149–218 mm, d = 0.98 mm; VICI metronics) containing benzene, toluene, and m-xylene revealed flow-dependent deviations between actual and certified emission rates. In a subsequent study, Susaya et al. (2012) investigated temperature variations between 30 and 100 °C, under two fixed nitrogen flow rates (400- and 800 mL-min^{-1}), observing 141 %, 87 %, and 85 % deviations in the emission rates of benzene, toluene, and m-xylene, respectively. Empirically determined actual emission rates across all tested PTs ranged from approximately 148 to 767 ng min^{-1} at 30 °C in the initial flow-dependence study and 188 to 88,265 ng min^{-1} in the temperature-dependence study (30–100 °C). Similarly, Kim et al. (2012) found that the actual emission rate of BTEX PTs housed in a glass impinger generator ranged approximately from 44.9 to 242.9 ng min^{-1} under nitrogen flows of 50–800 mL min^{-1} at 25 °C. Notably, none of these studies reported the time required to validate actual emission rates.

Furthermore, Aoyagi et al. (2017) collected generated gaseous acetaldehyde from a custom polyethylene PT (L = 100 mm, δ = 1 mm) under a 200 mL min^{-1} flow of nitrogen or zero-air onto DNPH cartridges, followed by HPLC-UV quantification. Validated emission rates (determined over 3 months) under nitrogen and zero-air flows were 2403±110 and 2469±113 ng min^{-1} at 10 °C, 6812±310 and 6682±305 ng min^{-1} at 20 °C, and 18 349±835 and 17 659±805 ng min^{-1} at 30 °C, respectively (uncertainties reported as expanded uncertainty (k = 2)). In a later study, Aoyagi et al. (2025) applied the same reference method to analyze emissions from a custom low-emission acetone PT (FEP, δ = 1.2 mm connected to a 6.5 cm-long stainless-steel reservoir of i.d. = 0.5 mm) operating under nitrogen flow. They reported acetone emission rates of 0.297±0.017, 0.409±0.011, and 0.677±0.020 ng min^{-1}, at 5, 10, and 15 °C, respectively (uncertainties reported as expanded uncertainty (k = 2)).

In another work, Grandjean et al. (2024) developed a portable temperature-controlled formaldehyde generator utilizing two paraformaldehyde PTs: PT1 (commercial) and PT2 (a 1/4" stainless-steel nut closed with PDMS membrane, δ = 1.5 × Ø = 9.7 mm, containing almost 100 mg of paraformaldehyde). Emission rates were obtained using the reference DNPH/HPLC-UV method under a nitrogen flow of 30–100 mL min^{-1} over a temperature range of 45–70 °C. Generated emission rates ranged from 3.09±0.18 ng min^{-1} to 14.09±0.66 ng min^{-1} between 50 and 65 °C for PT1 and from 178±13 ng min^{-1} to 1484±108 ng min^{-1} between 45 and 70 °C for PT2. Generated concentrations using PT1 stabilized within 1 h to reach 95 % of the final concentration (1.5 h for 99 %), and demonstrated 1-year long-term stability under 75 % continuous operation.

In comparison, the present work demonstrates rapid emission rate stabilization for multiple PTs, spanning diverse membrane materials and analytes of different chemical families, within 5 days from the onset of online TD-GC-FID monitoring at an initial temperature of 35 °C (see Fig. S1).

3.5.5 Spectroscopic calibration method versus the online TD-GC-FID based method

Neuman et al. (2003) reported using UV absorption spectroscopy at 185 nm to calibrate commercial HNO_3 and NH_3 PTs (stainless-steel reservoir with FEP membranes) under dry nitrogen gas at flow rates of 10–50 mL min^{-1} across temperatures from 30 to 45

https://doi.org/10.5194/egusphere-2026-4617
Preprint. Discussion started: 25 August 2026

°C (Neuman et al., 2003). Measured emission rates ranged from 13 to 150 ng min^{-1} (precision ±1 ng min^{-1}, accuracy ±10 %). Equilibrium stability was rapidly attained: less than 20 min was only required following a temperature step, approximately 30 min after adjusting the flow rate, and roughly 1 h after a pressure change. Stable emission rates were continuously monitored over periods extending from 3 months to 1 year.

3.5.6 On-line TD-GC-FID based method and quantification using the ECN approach

Neri et al. (2006) described an online GC-FID monitoring approach following serial gravimetric measurements (conducted over several days until the standard error reached a 95 % confidence level) using a microanalytical balance to calibrate two ethanol PTs: PT1 (wafer type, stainless-steel tank capped by a silicon membrane, d = 4.5 mm, Ø =1.5 mm) and PT2 (EL-type, stainless-steel tank capped with an exposed length of silicon membrane, L = 100 mm, d = 4.5 mm, δ = 1.5 mm) (Neri et al., 2006). The resulting ethanol emission rates at 20 °C were 3150 ng min^{-1} and 31,550 ng min^{-1}, respectively. They dynamically studied ethanol generation across a 1–500 ppm range in a temperature-compensated calibrator (18–28 °C), evaluating temperature impacts on the response (mV) of a GC-FID equipped with a real-time signal processing module.

In contrast, we report an advanced generation system coupled to an online TD-GC-FID capable of multiple temperature characterization across 25–120 °C. By utilizing multiple permeation ovens with room-temperature compensation alongside controlled dry zero-air carrier flows, several PTs can be evaluated simultaneously. This methodology shortens the calibration process of PTs, by eliminating the need to wait for thermal equilibration to room temperature prior to balance weighing, as well as removing the requirement for repeated weighings to establish a 95 % confidence interval. Indeed, the present work extends prior calibration frameworks into a versatile online methodology that accommodates a broader emission rate spectrum for diverse BVOCs—including aromatics, alcohols, aldehydes, and terpenes—while simplifying PT design, and enabling rapid, empirical concentration determinations. Compared with previously reported approaches, this platform offers greater flexibility regarding membrane selection, PT geometry, target analytes, carrier gas flow rates and operating temperature.

In addition, direct concentration quantification via online TD-GC-FID represents a major operational advantage. Offline measurement methods entail sequential collection, sampling, transport, handling, and analytical steps, resulting in significant delays before retrieving quantitative data to compute emission rates. Rapid online TD-GC-FID acquisition bypasses these delays through real-time concentration measurements, eliminating sample storage and handling steps. For example, offline DNPH-HPLC sampling introduces additional time-consuming chemical derivatization alongside multi-step processing protocols (Aoyagi et al., 2017, 2025; Grandjean et al., 2024), requiring several hours to a full day for batch preparation and analysis. In addition, our analytical device integrates an ambient-temperature focusing trap, avoiding the use of a separate adsorbent sampling tubes utilized in earlier studies (Kim et al., (2012); Susaya et al., (2011, 2012)).

Furthermore, we implement the effective carbon number (ECN) concept to rapidly quantify VOC concentrations lacking in certified commercial gas cylinders (see Sect. 2.5.1 and Table S2). By refining FID response factors based on this universal principle, the reliance on expensive, individual calibration standards is circumvented. This is particularly crucial for monoterpenes and oxygenated VOCs (OVOCs), which are notoriously unstable in compressed gas cylinders due to wall adsorption and chemical degradation. For example, in the NOMHICE intercomparison involving 29 laboratories (Apel et al., 1999), α-pinene exhibited the highest average systematic error (–40 %) among 57 evaluated compounds, suffering a 15 % underestimation of reference concentrations in cylinders over six weeks. Similarly, Rhoderick and Lin (2013) demonstrated that α-pinene and β-pinene concentrations decreased over time in conventional cylinders, whereas D-limonene, camphene, and p-cymene concentrations unexpectedly increased— signifying probable chemical isomerization to other monoterpenes rather than simple physical adsorption. Regarding OVOCs, Rhoderick et al. (2019) reported long-term wall losses even in specialized cylinders (e.g., –1.9 %

https://doi.org/10.5194/egusphere-2026-4617
Preprint. Discussion started: 25 August 2026

over 600 days for 2 ppm formaldehyde in Al-Acu-VIII-treated cylinder), and initial losses for acetaldehyde in Silco-treated stainless-steel cylinders. Consequently, long-term stability in cylinders demands specialized, analyte-specific surface passivations. Given these degradation issues and the presence of terpene transformation products during sampling, the ECN approach provides a reliable, robust alternative for accurately estimating generated VOC concentrations in direct alignment with NIST-traceable standards.

3.5.7 Permeability

Given the membrane dimensions, lateral surface area, and the $P_{VOC}(T)$ values at each investigated temperature, the apparent permeability coefficients Pr (T) of each membrane for each VOC_i were empirically derived from the experimentally calculated $ER_{VOC_i}(T)$ values at each temperature using Eq. (14) provided in Sect. 3.2. Independent of the PT geometry, the calculated Pr (T) values allowed for a direct comparison of membrane performance (PTFE vs. PDMS/PTFE) and analyte transport dynamics (benzene vs D-limonene, and *(E)*-2-hexenal vs. 2-methyl-1-butanol).

For the benzene–PTFE system, calculated Pr (T) coefficients ranged from 4.13×10^{-12} to 5.86×10^{-12} mol m^{-1} s^{-1} Pa^{-1} across 35–50 °C (see Table S13). Over the same temperature range, D-limonene Pr (T) values increased progressively from 3.85×10^{-13} to 4.89×10^{-13} mol m^{-1} s^{-1} Pa^{-1}. Thus, benzene apparent permeabilities are approximately 10 to 15 times higher than those of D-limonene. The difference is primarily attributed to the larger molecular size and the bulkier chemical structure of D-limonene, which restricts its diffusion through the PTFE matrix. Nevertheless, variations in solubility coefficients S may also contribute directly related to the observed magnitude differences. To the best of our knowledge, explicit diffusion (D_i) and solubility (S) values for the benzene–PTFE and D-limonene–PTFE systems have not been previously reported in the literature. Consequently, these values represented a qualitative explanation of this difference between the two systems based on $\mathrm{Pr}(T) = D_i \times \mathrm{S}$.

The apparent Pr (T) values for *(E)*-2-hexenal–PDMS/PTFE system reflect combined transport resistance through a 2 mm PDMS membrane (in direct contact with the liquid reservoir), superimposed with a 2 mm PTFE membrane. Consequently, the derived values represent the effective permeability in a binary stacked PDMS/PTFE membrane system (δ_{total} = 4 mm) (Table S14).

Across 25–40°C, the apparent Pr (T) values ranged between 1.58×10^{-9} and 2.36×10^{-9} mol m^{-1} s^{-1} Pa^{-1} for *(E)*-2-hexenal–PDMS/PTFE system, and between 1.68×10^{-9} and 1.97×10^{-10} mol m^{-1} s^{-1} Pa^{-1} for the 2-methyl-1-butanol–PDMS/PTFE system. This demonstrates an 8- to 14-fold higher permeability for *(E)*-2-hexenal compared to 2-methyl-1-butanol across the investigated temperature range. Because PDMS serves as the primary membrane in direct contact with the liquid phase, solubility dominates diffusivity in governing overall transport in this PT architecture. The hydrophobic nature of PDMS, imparted by nonpolar methyl groups (─CH_3) in its backbone, retards the partitioning and transport of 2-methyl-1-butanol to the top PTFE layer. Conversely, faster solubilization and stronger partitioning of *(E)*-2-hexenal into the PDMS matrix yield significantly higher apparent permeability coefficients.

An extensive literature review revealed that experimental permeability coefficients for such dual-membrane or specific BVOC systems are extremely scarce. Therefore, this work provides the first experimental permeability data for the four determined for the four studied compounds of different chemical classes across membrane configurations, and temperatures.

While true permeability coefficients are conventionally measured electrochemically, via direct differential permeation method, or through indirect sorption measurements (Davis et al., 2004; Dobson and Taylor, 1986; Friess et al., 2004), our approach enables direct computation of the Pr (T) values directly from TD-GC-FID emission rate measurements, without requiring separate diffusion or sorption devices. Decoupled insights into diffusion and sorption can subsequently be inferred to optimize permeation system for other compounds within the same chemical family.

https://doi.org/10.5194/egusphere-2026-4617
Preprint. Discussion started: 25 August 2026

3.5.8 Range of generated concentrations

The custom-designed PTs in this work generated concentrations spanning an overall range extending from low ppb (1.2 ppb) up near ppm levels (956 ppb, i.e., 0.96 ppm) under the investigated conditions. This wide concentration range allows for the calibration of generators producing various trace-level calibration standards relevant to atmospheric and plant-emission studies. Although these concentrations are typically higher than ambient atmospheric levels, they are exceptionally well-suited for the validation of generators' performance over a reproducible dynamic range. Table S12 illustrates how concentration ranges vary according to the target application, from sub-ppb or ppt levels for atmospheric trace measurements to high-ppm levels for sensor calibration and laboratory validation.

We established a direct comparison for the benzene PT, as it is widely used across numerous applications and operating conditions reported in the literature. For benzene, the measured concentration range (149.9–661.6ppb) under the investigated conditions agreed well with previously reported literature, which spans over 0.56–2.04 orders of magnitude (0.25–69.2 ppm on average) (Kim et al., 2012; Susaya et al., 2012). To our current knowledge, no published studies have previously demonstrated the generation of *(E)*-2-hexenal gaseous standard using permeation technology. As a primary green leaf volatile (GLV) aldehyde, *(E)*-2-hexenal can instead be compared with other aldehydic species previously generated by PTs, such as formaldehyde and acetaldehyde. Reported formaldehyde (HCHO) permeation systems from low ppb (~7 ppb) up to high ppb levels (~380 ppb) for low-emitting HCHO PTs, and reach over 40 ppm for high-emitting configurations (Grandjean et al., 2022, 2024). In contrast, no explicit concentration ranges were provided by Aoyagi et al. (2017), regarding acetaldehyde (CH_3CHO) generation. In terms of chemical stability, *(E)*-2-hexenal is inherently less stable than HCHO and CH_3CHO, because of its α, β-unsaturated aldehydic structure. As a result, generating stable streams of this particular aldehyde presented a major challenge, even within the targeted high-ppb to ppm range (496–956 ppb).

Similarly, no permeation devices were previously calibrated for 2-methyl-1-butanol, precluding a direct comparison of generated concentrations with literature data. However, as an oxygenated alcohol, its permeation behavior is to that of ethanol. Neri et al. (2006) reported ethanol PTs generating 1–500 ppm, intended primarily for temperature-compensated sensor calibration. Our lower concentration range of 0.3–1.2 ppm is better suited for analytical applications involving biological or atmospheric studies of trace BVOCs, providing a new methodology for generating relevant alcohols with high specificity.

Regarding D-limonene, as a representative of monoterpene, it is more instructively compared with alternative terpene generation techniques. Terpene generation via permeation technology remains limited due to extremely low diffusion coefficients (Pr (*T*) ranged from 3.85×10^{-13} to 4.89×10^{-13} mol m^{-1} s^{-1} Pa^{-1} between 30 °C and 50°C) and high susceptibility to oxidation and adsorptive losses. For example, Komenda et al. (2001) used D-limonene as a standard solely within a diffusion cell to generate a complex BVOC mixture (terpenes, oxygenated terpenes, aldehydes) for GC-FID calibration, achieving a total mixture concentration range of 0.5–750 ppb. Iqbal and Kim (2014) developed a dynamic headspace extraction technique by sweeping liquid standards of 10 BVOCs (including D-limonene) with 100 mL min^{-1} pure nitrogen, yielding steady-state concentrations of 0.34–6.92 ppb following sorbent tube collection. In comparison, our D-limonene PT produced concentrations between 1.2 and 550.2 ppb, demonstrating strong consistency with these alternative techniques.

Although operating conditions generated concentrations predominantly in the upper ppb range, this does not constraint the system's ability to reach sub-ppb levels if MFC3 operates at its maximum capacity (see Fig. 2) or if the temperature of the permeation oven is decreased. Using the experimental emission rates, theoretical concentration ranges were calculated using Eq. (6) at minimum (no dilution, upper bound) and maximum MFC3 capacity (1000 mL min^{-1} dry zero-air, lower bound). We report extrapolated concentration ranges of 78.3–2547.6 ppb for benzene (25–50 °C), 263.2–2547.6 ppb for *(E)*-2-hexenal (25–40 °C), 83.4–2143.1 ppb for 2-methyl-1-butanol (25–45 °C), and 0.5–2209.6 ppb for D-limonene (35–120 °C) (Table S11). In previous work, Bachelier

https://doi.org/10.5194/egusphere-2026-4617
Preprint. Discussion started: 25 August 2026

et al. (2024) demonstrated through, linearity tests that an automated TD-GC-FID/MS system, operating on similar principles, could reliably quantify concentration down to detection limits of 20 ppt (benzene), 23 ppt (α-pinene), and 130 ppt (isopropyl alcohol) among many other alkanes, aromatic hydrocarbons, OVOCs, and halogenated compounds.

4 Conclusions

Accurate quantification of gaseous VOCs in atmospheric and biological applications requires the use of advanced analytical instrumentation. To ensure the analytical validity of these measurements, reliable calibration standards are paramount; however, conventional gas cylinders present significant drawbacks, including high cost and limited long-term stability. In this study, we developed novel permeation devices for BVOCs whose applicability in polymeric systems (PTFE and PDMS) had not been previously documented. Concentration ranges extending from low ppb up to low ppm were generated with high precision (RSD <20 % with a maximum RSD of 16.6 %, 2-methyl-1-butanol) by integrating a dilution system that minimizes carrier gas consumption. The dynamic, multi-temperature generation strategy (25–120 °C) enabled the comprehensive characterization of permeation tubes using continuous online TD-GC-FID analyses, significantly reducing calibration time compared to traditional gravimetric or offline methods. Rapid initial concentration stabilization was achieved within less than two weeks, offering a distinct advantage over conventional gravimetric techniques for field-deployable applications, such as plant-emission profiling or atmospheric monitoring.

It was demonstrated that the emission rate of each permeation device was independent of the matrix gas flow rate, but strongly governed by temperature over the 25–120 °C range. This thermal dependence followed combined thermodynamic and transport relationships derived from Antoine's law and Fick's law of diffusion (R^2>0.922). Experimentally validating these relations allowed for the determination of apparent permeability coefficients (10^{-13}–10^{-9}) providing fundamental insights into analyte–polymer membrane interactions independent of device geometry. This further confirmed that analyte transport in these systems is purely permeation-driven, demonstrating that potential leak artifacts are negligible.

An important asset of this setup is the implementation of the Effective Carbon Number (ECN) concept, which provides a fast and simple universal calibration method based on FID response factors, carbon number and heteroatoms functionality relative to a single reference compound. By combining this ECN approach with custom-designed permeation devices, the reliance on high-pressure compressed cylinders is significantly reduced, offering a cost-effective and flexible alternative for in-house standard generation.

With the help of the predictable FID response, TD-GC-FID devices can pave the way for calibrating alternative detectors dedicated to organic species, such as photoionization detectors (PIDs) used for monitoring biogenic compounds, aromatics, or hazardous air pollutants (HAPs). Indeed, GC-PID suffers from a sensitivity drift over time that requires regular monitoring. Furthermore, response factors are not known for all VOCs. Given the modest number of measurements required to generate highly repeatable, multi-component gas streams in a compact system, this platform is well-suited for future routine sensor calibration and laboratory validation. Finally, further predictive modelling could leverage these quantitative relationships to directly link the physicochemical properties of target BVOCs with polymer membrane specifications and permeation tube geometries.

https://doi.org/10.5194/egusphere-2026-4617
Preprint. Discussion started: 25 August 2026

Data availability

A substantial part of the underlying research data and supplementary figures/tables are provided in the Supplementary Material accompanying this article. All additional raw data and datasets used in this study are available from the corresponding author upon reasonable request.

Supplement link

The link to the supplement will be included by Copernicus, if applicable.

Author contributions

AG designed and carried out all the experiments with the support of SLC, DB, and MM. AG performed all the analyses and data processing. SLC and DB supervised the study and validated the uncertainty calculations. JPA and DB secured the funding and supplied the resources required to carry the experimental work. AG prepared the original draft of the manuscript, which was thoroughly revised by SLC. All authors commented on the manuscript.

Competing interests

The authors declare that they have no conflict of interest.

Acknowledgements

The authors gratefully acknowledge Pierre Dupuy and Marine Patuel for their valuable technical assistance, as well as Marie-Claude Lacoste, Agnès Gabard, and Alexandre Pauly for their support during the calibration and initialization of the developed generation system at Chromatotec.

Financial support

This work was supported by Chromatotec (Saint-André-de-Cubzac, France) in collaboration with ICPEES (Strasbourg, France) under PurPest project (grant number 101060634, 2023). PurPest project is funded by the European Union. Views and opinions expressed are however those of the author(s) only and do not necessarily reflect those of the European Union or the European Research Executive Agency. Neither the European Union nor the granting authority can be held responsible for them.

Review statement

The review statement will be added by Copernicus Publications listing the handling editor as well as all contributing referees according to their status anonymous or identified.

https://doi.org/10.5194/egusphere-2026-4617
Preprint. Discussion started: 25 August 2026

References

Amiet, F., Vivola, L., Bazin, D., and Gutiérrez-Sama, S.: Development of on-line and Field Dual TD-GC-FID/MS for Automatic and Continuous Volatile Organic Compounds (VOCs) Ambient Air and Odour Monitoring, Chem. Eng. Trans., 68, 271–276, https://doi.org/10.3303/CET1868046, 2018.

Aoyagi, R., Ikeda, S., Kaifuku, Y., Matsunobu, K., and Sekine, Y.: Investigation on stability of acetaldehyde standard gas generated with the permeation tube method, Indoor Environment, 20, 3–10, https://doi.org/10.7879/SIEJ.20.3, 2017.

Aoyagi, R., Arakawa, T., Iitani, K., Mitsubayashi, K., Sekine, Y., and Kaifuku, Y.: Development of dynamic gas generation system for ultratrace amounts of acetone at parts-per-trillion levels with low temperature permeation method, Discover Applied Sciences, 7, 1–11, https://doi.org/10.1007/s42452-025-06722-x, 2025.

Atkinson, R.: Atmospheric chemistry of VOCs and NOx, Atmos. Environ., 34, 2063–2101, https://doi.org/10.1016/S1352-2310(99)00460-4, 2000.

Atkinson, R. and Arey, J.: Atmospheric Degradation of Volatile Organic Compounds, Chem. Rev., 103, 4605–4638, https://doi.org/https://doi.org/10.1021/cr0206420, 2003.

Bachelier, F., Mascles, M., McGillen, M. R., Amiet, J. P., Grosselin, B., Bazin, D., and Daële, V.: Development, optimization and validation of automated volatile organic compound data analysis using an on-line thermal desorption gas chromatograph with dual detection and application to measurements in ambient air, J. Chromatogr. A, 1735, 465327, https://doi.org/10.1016/J.CHROMA.2024.465327, 2024.

Bankovich, P. W. and Modrell, R. W.: Preparation of vinyl chloride standards using a permeation tube, Am. Ind. Hyg. Assoc. J., 37, 640–646, https://doi.org/10.1080/0002889768507537, 1976.

De Blas, M., Navazo, M., Alonso, L., Durana, N., and Iza, J.: Automatic on-line monitoring of atmospheric volatile organic compounds: Gas chromatography–mass spectrometry and gas chromatography–flame ionization detection as complementary systems, Science of The Total Environment, 409, 5459–5469, https://doi.org/10.1016/J.SCITOTENV.2011.08.072, 2011.

Braun, J., Engelhard, C., and Kaul, P.: Optimized fast gas chromatography coupled with proton-transfer-reaction time-of-flight mass spectrometry for the selective near real-time analysis of herbivore-induced plant volatiles, J. Chromatogr. A, 1759, 466236, https://doi.org/10.1016/J.CHROMA.2025.466236, 2025.

Cedergren, A. and Fredriksson, S. Å.: Trace analysis for chlorinated hydrocarbons in air by quantitative combustion and coulometric chloride determination: Application to standardization of vinyl chloride permeation tubes, Talanta, 23, 217–223, https://doi.org/10.1016/0039-9140(76)80172-5, 1976.

Coatsworth, P., Gonzalez-Macia, L., Collins, A. S. P., Bozkurt, T., and Güder, F.: Continuous monitoring of chemical signals in plants under stress, Nature Reviews Chemistry 2022 7:1, 7, 7–25, https://doi.org/10.1038/s41570-022-00443-0, 2022.

Crescentini, G., Mangani, F., Mastrogiacomo, A. R., and Bruner, F.: Calibration method for the gas chromatographic analysis of halocarbons in atmospheric samples using permeation tubes and an electron-capture detector, J. Chromatogr. A, 204, 445–451, https://doi.org/10.1016/S0021-9673(00)81691-X, 1981.

Davis, P. K., Lundy, G. D., Palamara, J. E., Duda, J. L., and Danner, R. P.: New Pressure-Decay Techniques to Study Gas Sorption and Diffusion in Polymers at Elevated Pressures, Ind. Eng. Chem. Res., 43, 1537–1542, https://doi.org/10.1021/IE034075Y/ASSET/IMAGES/LARGE/IE034075YF00004.JPEG, 2004.

Dietz, R. N., Cote, E. A., and Smith, J. D.: New Method for Calibration of Permeation Wafer and Diffusion Devices, Anal. Chem., 46, 1974.

Dobson, J. V. and Taylor, M. J.: Electrochemically derived values of the permeability coefficient of common gases through PTFE membranes between 9 and 41°C, Electrochim. Acta, 31, 235–239, https://doi.org/10.1016/0013-4686(86)87114-6, 1986.

Faiola, C. L., Erickson, M. H., Fricaud, V. L., Jobson, B. T., and Vanreken, T. M.: Quantification of biogenic volatile organic compounds with a flame ionization detector using the effective carbon number concept, Atmos. Meas. Tech., 5, 1911–1923, https://doi.org/10.5194/AMT-5-1911-2012, 2012.

Friess, K., Šípek, M., Hynek, V., Sysel, P., Bohatá, K., and Izák, P.: Comparison of permeability coefficients of organic vapors through non-porous polymer membranes by two different experimental techniques, J. Memb. Sci., 240, 179–185, https://doi.org/10.1016/J.MEMSCI.2004.05.006, 2004.

https://doi.org/10.5194/egusphere-2026-4617
Preprint. Discussion started: 25 August 2026

Grandjean, A., Bazin, D., Amiet, F., and Le Calvé, S.: Comparison of Two Analytical Systems for Continuous Monitoring of Ppb to Ppm-levels of Formaldehyde in Air, Chem. Eng. Trans., 95, 67–72, https://doi.org/10.3303/CET2295012, 2022.

Grandjean, A., Becker, A., Kustner, C., Wolf, M., Sutter, C., Severac, R., Amiet, J. P., Bazin, D., and Le Calvé, S.: Portable temperature-controlled permeation device for the generation of formaldehyde gas standard, Microchemical Journal, 206, https://doi.org/10.1016/j.microc.2024.111544, 2024.

Guenther, A.: Biological and Chemical Diversity of Biogenic Volatile Organic Emissions into the Atmosphere, ISRN Atmospheric Sciences, 2013, 1–27, https://doi.org/10.1155/2013/786290, 2013.

Guenther, A., Hewitt, C. N., Erickson, D., Fall, R., Geron, C., Graedel, T., Harley, P., Klinger, L., Lerdau, M., Mckay, W. A., Pierce, T., Scholes, B., Steinbrecher, R., Tallamraju, R., Taylor, J., and Zimmerman, P.: A global model of natural volatile organic compound emissions, Journal of Geophysical Research: Atmospheres, 100, 8873–8892, https://doi.org/10.1029/94JD02950, 1995.

Guillevic, M., Vollmer, M. K., Wyss, S. A., Leuenberger, D., Ackermann, A., Pascale, C., Niederhauser, B., and Reimann, S.: Dynamic-gravimetric preparation of metrologically traceable primary calibration standards for halogenated greenhouse gases, Atmos. Meas. Tech., 11, 3351–3372, https://doi.org/10.5194/AMT-11-3351-2018, 2018.

International Organization for Standardization (ISO): Gas analysis — Preparation of calibration gas mixtures using dynamic volumetric methods — Part 10: Permeation method, Geneva, Switzerland, 2002.

Iqbal, M. A. and Kim, K. H.: Generation of sub-ppb level vapor phase mixtures of biogenic volatile organic compounds from liquid phase standards and stepwise characterization of their volatilization properties by thermal desorption-gas chromatography-mass spectrometry, J. Chromatogr. A, 1373, 149–158, https://doi.org/10.1016/j.chroma.2014.10.086, 2014.

Jorgensen, A. D., Picel, K. C., and Stamoudis, V. C.: Prediction of gas chromatography flame ionization detector response factors from molecular structures, Analytical Chemistry (Washington); (USA), 62:7, 683–689, https://doi.org/10.1021/AC00206A007, 1990.

Kállai, M. and Balla, J.: The effect of molecular structure upon the response of the flame ionization detector, Chromatographia, 56, 357–360, https://doi.org/10.1007/BF02491945, 2002.

Kállai, M., Veres, Z., and Balla, J.: Response of flame ionization detectors to different homologous series, Chromatographia, 54, 511–517, https://doi.org/10.1007/BF02491209, 2001.

Kesselmeier, J. and Staudt, M.: Biogenic volatile organic compounds (VOC): An overview on emission, physiology and ecology, J. Atmos. Chem., 33, 23–88, https://doi.org/10.1023/A:1006127516791/METRICS, 1999.

Ketola, R. A., Kiuru, J. T., Tarkiainen, V., Kokkonen, J. T., Räsänen, J., and Kotiaho, T.: Detection of volatile organic compounds by temperature-programmed desorption combined with mass spectrometry and Fourier transform infrared spectroscopy, Anal. Chim. Acta, 562, 245–251, https://doi.org/10.1016/J.ACA.2006.01.069, 2006.

Kim, K. H., Susaya, J., Cho, J., and Parker, D.: The combined application of impinger system and permeation tube for the generation of volatile organic compound standard gas mixtures at varying diluent flow rates, Sensors (Switzerland), 12, 10964–10979, https://doi.org/10.3390/s120810964, 2012.

Knopf, D.: Continuous dynamic-gravimetric preparation of calibration gas mixtures for air pollution measurements, 113–119 pp., 2001.

Lara-Ibeas, I., Rodríguez-Cuevas, A., Andrikopoulou, C., Person, V., Baldas, L., Colin, S., and Calvé, S. Le: Sub-ppb level detection of BTEX Gaseous mixtures with a compact prototype GC equipped with a preconcentration unit, Micromachines (Basel)., 10, https://doi.org/10.3390/mi10030187, 2019.

Lee, C., Kim, Y. J., Hong, S. B., Lee, H., Jung, J., Choi, Y. J., Park, J., Kim, K. H., Lee, J. H., Chun, K. J., and Kim, H. H.: Measurement of atmospheric formaldehyde and monoaromatic hydrocarbons using differential optical absorption spectroscopy during winter and summer intensive periods in Seoul, Korea, Water Air Soil Pollut., 166, 181–195, https://doi.org/10.1007/S11270-005-7308-6/METRICS, 2005.

Li, M. W.-H., Ghosh, A., Venkatasubramanian, A., Sharma, R., Huang, X., and Fan, X.: High-Sensitivity Micro-Gas Chromatograph-Photoionization Detector for Trace Vapor Detection, ACS Sens., 6, 2348–2355, https://doi.org/10.1021/acssensors.1c00482, 2021.

Liaud, C., Nguyen, N. T., Nasreddine, R., and Le Calvé, S.: Experimental performances study of a transportable GC-PID and two thermo-desorption based methods coupled to FID and MS detection to assess BTEX exposure at sub-ppb level in air, Talanta, 127, 33–42, https://doi.org/10.1016/J.TALANTA.2014.04.001, 2014.

https://doi.org/10.5194/egusphere-2026-4617
Preprint. Discussion started: 25 August 2026

Macé, T., Iturrate-Garcia, M., Pascale, C., Niederhauser, B., Vaslin-Reimann, S., and Sutour, C.: Air pollution monitoring: development of ammonia (NH3) dynamic reference gas mixtures at nanomoles per mole levels to improve the lack of traceability of measurements, Atmos. Meas. Tech., 15, 2703–2718, https://doi.org/10.5194/AMT-15-2703-2022, 2022.

Maleknia, S. D., Bell, T. L., and Adams, M. A.: PTR-MS analysis of reference and plant-emitted volatile organic compounds, Int. J. Mass Spectrom., 262, 203–210, https://doi.org/10.1016/J.IJMS.2006.11.010, 2007.

Maria, P. C., Gal, J. F., Balza, M., Peré-Trepat, E., Tumbiolo, S., and Couret, J. M.: Using thermogravimetry for weight loss monitoring of permeation tubes used for generation of trace concentration gas standards, Anal. Chem., 74, 305–307, https://doi.org/10.1021/ac0108921, 2002.

Neri, G., Bonavita, A., Rizzo, G., Micali, G., Donate, N., and Ipsale, S.: Investigation of permeation tubes for temperature-compensated gas-sensor calibrators, IEEE Sens. J., 6, 1120–1124, https://doi.org/10.1109/JSEN.2006.881347, 2006.

Neuman, J. A., Ryerson, T. B., Huey, L. G., Jakoubek, R., Nowak, J. B., Simons, C., and Fehsenfeld, F. C.: Calibration and evaluation of nitric acid and ammonia permeation tubes by UV optical absorption, Environ. Sci. Technol., 37, 2975–2981, https://doi.org/10.1021/ES026422L/ASSET/IMAGES/LARGE/ES026422LF00008.JPEG, 2003.

O'Keeffe, A. E. and Ortman, G. C.: Primary Standards for Trace Gas Analysis, Anal. Chem., 38, 1966.

Peñuelas, J. and Llusià, J.: The complexity of factors driving volatile organic compound emissions by plants, Biol. Plant., 44, 481–487, https://doi.org/10.1023/A:1013797129428/METRICS, 2001.

Pérez Ballesta, P., Baldan, A., and Cancelinha, J.: Atmosphere Generation System for the Preparation of Ambient Air Volatile Organic Compound Standard Mixtures, Anal. Chem., 71, 2241–2245, https://doi.org/10.1021/AC981291L, 1999.

Purdue, L. J. and Thompson, R. J.: A Rapid, Sensitive Method for Calibration of Permeation Devices, Anal. Chem., 44, 1034–1036, https://doi.org/10.1021/AC60314A053/ASSET/AC60314A053.FP.PNG_V03, 1972.

Rhoderick, G. C. and Lin, J.: Stability assessment of gas mixtures containing monoterpenes in varying cylinder materials and treatments, Anal. Chem., 85, 4675–4685, https://doi.org/10.1021/AC400324V/SUPPL_FILE/AC400324V_SI_001.PDF, 2013.

Rhoderick, G. C., Cecelski, C. E., Miller, W. R., Worton, D. R., Moreno, S., Brewer, P. J., Viallon, J., Idrees, F., Moussay, P., Kim, Y. D., Kim, D., Lee, S., Baldan, A., and Li, J.: Stability of gaseous volatile organic compounds contained in gas cylinders with different internal wall treatments, Elementa, 7, https://doi.org/10.1525/ELEMENTA.366, 2019.

Saltzman, B. E., Burg, W. R., and Ramaswamy, G.: Performance of Permeation Tubes as Standard Gas Sources, Environ. Sci. Technol., 5, 1121–1128, https://doi.org/10.1021/ES60058A004/ASSET/ES60058A004.FP.PNG_V03, 1971.

Scanlon, J. T. and Willis, D. E.: Calculation of flame ionization detector relative response factors using the effective carbon number concept, J. Chromatogr. Sci., 23, 333–340, https://doi.org/10.1093/CHROMSCI/23.8.333, 1985.

Scaringelli, F. P., O'Keeffe, A. E., Rosenberg, E., and Bell, J.: Preparation of Known Concentrations of Gases and Vapors with Permeation Devices Calibrated Gravimetrically, Anal. Chem., 42, 871–876, 1970.

Seco, R., Peñuelas, J., and Filella, I.: Short-chain oxygenated VOCs: Emission and uptake by plants and atmospheric sources, sinks, and concentrations, Atmos. Environ., 41, 2477–2499, https://doi.org/10.1016/j.atmosenv.2006.11.029, 2007.

Sindelarova, K., Granier, C., Bouarar, I., Guenther, A., Tilmes, S., Stavrakou, T., Müller, J.-F., Kuhn, U., Stefani, P., and Knorr, W.: Global data set of biogenic VOC emissions calculated by the MEGAN model over the last 30 years, Atmos. Chem. Phys., 14, 9317–9341, https://doi.org/10.5194/acp-14-9317-2014, 2014.

Singh, H. B., Salas, L., Lillian, D., Arnts, R. R., and Appleby, A.: Generation of Accurate Halocarbon Primary Standards with Permeation Tubes, Environ. Sci. Technol., 11, 511–513, https://doi.org/10.1021/ES60128A009, 1977.

Sternberg, J., Gallaway, W., and Jones, D.: The mechanism of response of flame ionization detectors, in: Gas chromatography: third international symposium, edited by: Brenner, N., Callen, J. E., and Weiss, M. D., Academic Press, New York, NY, 231–267, 1962.

Stevens, R. K., O'Keeffe, A. E., and Ortman, G. C.: Absolute calibration of a flame photometric detector to volatile sulfur compounds at sub-part-per-million levels, Environ. Sci. Technol., 3, 652–655, https://doi.org/10.1021/ES60030A005, 1969.

Susaya, J., Kim, K. H., Cho, J. W., and Parker, D.: The use of permeation tube device and the development of empirical formula for accurate permeation rate, J. Chromatogr. A, 1218, 9328–9335, https://doi.org/10.1016/j.chroma.2011.11.007, 2011.

https://doi.org/10.5194/egusphere-2026-4617
Preprint. Discussion started: 25 August 2026

Susaya, J., Kim, K. H., Cho, J., and Parker, D.: The controlling effect of temperature in the application of permeation tube devices in standard gas generation, J. Chromatogr. A, 1225, 8–16, https://doi.org/10.1016/j.chroma.2011.12.066, 2012.

Tong, H. Y. and Karasek, F. W.: Flame Ionization Detector Response Factors for Compound Classes in Quantitative Analysis of Complex Organic Mixtures, Anal. Chem., 56, 2124–2128, https://doi.org/10.1021/AC00276A033/ASSET/AC00276A033.FP.PNG_V03, 1984.

Tumbiolo, S., Vincent, L., Gal, J. F., and Maria, P. C.: Thermogravimetric calibration of permeation tubes used for the preparation of gas standards for air pollution analysis, Analyst, 130, 1369–1374, https://doi.org/10.1039/b508536e, 2005.

U.S. Environmental Protection Agency (EPA): Compendium Method TO-17: Determination of Volatile Organic Compounds in Ambient Air Using Active Sampling onto Sorbent Tubes, Cincinnati, Ohio, USA, 1999.